Received: 23 May 2021 | Revised: 21 July 2021 | Accepted: 26 August 2021

DOI: 10.1002/cta.3139

ORIGINAL PAPER

WILEY

# A generalized model of coupled oscillator phase-noise response

**Torsten Djurhuus** | **Viktor Krozer**

Institute of Physics, Goethe-University Frankfurt, Frankfurt, Germany

**Correspondence**
Torsten Djurhuus, Institute of Physics, Goethe-University Frankfurt, Max-von-Laue-Str. 1, 60438 Frankfurt, Germany.
Email: t.djurhuus@physik.uni-frankfurt.de

**Funding information**
German Research Foundation, Grant/Award Number: KR 1016/16-1

**Summary**

Model frameworks, based on Floquet theory, have been shown to produce effective tools for accurately predicting phase-noise response of single (free-running) oscillator systems. This method of approach, referred to herein as macro-modeling, has been discussed in several highly influential papers and now constitutes an established branch of modern circuit theory. The increased application of, for example, injection-locked oscillators and oscillator arrays in modern communication systems has subsequently exposed the demand for similar rigorous analysis tools aimed at coupled oscillating systems. This paper presents a novel solution in terms of a macro-model characterizing the phase-response of synchronized coupled oscillator circuits and systems perturbed by weak noise sources. The framework is generalized and hence applicable to all circuit configurations and coupling topologies generating a synchronized steady-state. It advances and replaces the phenomenological descriptions currently found in the published literature pertaining to this topic and, as such, represents a significant breakthrough *w.r.t.* coupled oscillator noise modeling. The proposed model is readily implemented numerically using standard routines.

**KEYWORDS**

circuit analysis, coupled oscillators, Floquet theory, nonlinear dynamical systems, oscillators, phase noise, synchronized oscillators, system analysis and design

## 1 | INTRODUCTION

Rigorous phase-noise modeling tools represent a critical part of accessing the performance of any system involving oscillators/clocks operating at, or around, room temperature.[1–4] The state of time-domain oscillator noise modeling has evolved over the years culminating with the invention of phase-noise macro-model (PMM), first proposed by Kärtner[5] and later further developed and refined by Demir et al. as well by other research groups including the authors of this paper.[6–8] Herein, the term *macro-model* is introduced as a handle to refer to the category of Floquet-theory-based methodologies discussed in other studies.[5–7] The PMM delivers a rigorous, coordinate independent description which is the objectively correct mathematical solution approach to the presented problem. As such, it basically answers all open questions, and its development has hence effectively closed the

book on single (free-running) oscillator time-domain noise modeling; the field has reached maturity. In contrast, the topic of time-domain coupled oscillator macro-modeling is still very much in its infancy despite several important practical applications in modern communication and sensing systems such as beam-steering arrays and injection-locked low-power synthesizers. Below, we refer to the synchronized coupled oscillator circuit class/category by the C-OSC label. In contrast, the single (free-running), oscillator class/category will be assigned to the S-OSC label.

The work described herein concerns the proposal of a novel macro-model for predicting the stochastic phase-response of noise-perturbed C-OSC electronic ensembles operating at, or around, room temperature. The proposed C-OSC PMM is fully generalized and can be applied to any type of synchronized system irrespective of the specific details such as circuit/coupling topology, state dimension, and parameter dependence. The C-OSC framework, described herein, furthermore directly reduces to the previously proposed S-OSC description in other studies[5–7] for the trivial case of a single oscillator ensemble (free-running oscillator with no coupling), that is, the proposed C-OSC PMM implicitly contains the S-OSC PMM as a special case.

## 1.1 | Motivation and summary of main results

Clock devices are often implemented through the coupling of two or several free-running oscillator units since synchronization in these C-OSC configurations represent a power-efficient alternative to more elaborate phase-locked systems. Examples of specific C-OSC applications include low-power frequency multipliers/dividers,[9] nonlinear noise filters,[10,11] antenna beam steering,[12–15] low-power high-frequency synthesizer solutions,[16] and efficient power combining units[17,18]; to mention but a few examples. Given the right conditions, a C-OSC ensemble of $k$-coupled autonomous oscillator circuits, a *k-order ensemble*, will synchronize and oscillate at a single common frequency. The asymptotic dynamics of such synchronized ensemble is then characterized by a single periodic steady-state (PSS). In PSS systems, the most important consequence of weak-noise perturbations is the generation of *jitter* in the steady-state phase, that is, *phase-noise*. This issue is directly responsible for the spectral broadening observed in all physical oscillator/clock devices. The jitter/phase-noise broadening of the spectrum presents a significant practical problem as it, for example, causes interchannel interference in communication systems which in-turn results in increased bit error rates (BER). Minimizing the bandwidth of oscillator/clock spectra remains one of the most critical aspects modern optical and electronic communication system design and represents the main bottleneck obstructing optimized performance.[5,6,19]

Given the importance of this topic, phase-noise modeling of C-OSC systems has been the focus of several research efforts over the years (see, e.g., other studies[17,20–24]). The modeling strategies described in these works, and others of the same category, are all based on phenomenological and/or block-diagram formulations. This approach to modeling limits the scope of application to a specific category of systems, that is, one model may apply to quasi-harmonic oscillators coupled bilaterally, whereas another concerns ring oscillators coupled unilaterally. The approach furthermore inevitably introduces additional extraneous parameters (e.g., resonator Q-factor and amplitude saturation coefficient) and does not allow for implementation of general purpose numerical solutions. Finally, such phenomenological modeling strategies can lead to results which predict nonphysical behavior. A well-known example hereof is the frequency-domain conversion-matrix (FD-CM) method, currently being used in at-least one of the leading commercial CAD simulator programs presently on the market, which famously predicts a phase-noise spectrum that blows-up (i.e., has a singularity) at zero frequency offset from carrier.[6] The novel C-OSC PMM proposed herein is based on a rigorous theoretic description developed directly from the core underlying stochastic differential equation (SDE) model. This approach corrects all of the issues described above.

Both S-OSC and C-OSC (synchronized) systems are governed dynamically by the presence of a PSS (limit-cycle), and it is hence natural to ask: Can we simply re-use the S-OSC PMM, developed previously in other studies,[5–7] to predict the C-OSC phase-noise response? The answer to this question is an unequivocal no! Consider the special C-OSC subclass of *injection-locked oscillators* (INJ-OSC) involving one-way, unilateral, coupling of two oscillator units. It is an established fact, verified experimentally,[10,25,26] that the phase-noise spectrum of an INJ-OSC system does not correspond to the Lorentzian template prescribed by the S-OSC PMM but instead has a more complex form involving additional zeros and poles. A completely new theory of C-OSC phase-noise dynamics is required to capture this spectrum.

## 1.2 | Paper summary

Following a brief introduction to various topics and concepts, relevant to our discussion S, the existence of a so-called *phase-manifold*, $\mathcal{P}$, is proven (Section 3). To achieve this result, we apply the well-established theory on persistence of normally hyperbolic (NH) manifolds.[27–30] A phase-amplitude coordinate representation is then introduced to parameterize this space (Section 4) and, invoking the weak-noise assumption, the stochastic phase-noise response is calculated (Section 5). A brief summary of the model developed in Sections 2–5 takes the form: *the stochastic phase-response (weak noise), of a k-order C-OSC ensemble, is governed by k unique Floquet modes; the so-called phase-modes*. Using this novel insight, the following expression C-OSC single-sided phase-noise spectrum is derived in Section 6

$$\mathfrak{L}(\omega_m)=\frac{(1-a^{(1)})(\omega_0^2 c)-2b^{(1)}\omega_m}{(0.5\omega_0^2 c)^2+\omega_m^2}+\sum_{\rho=-\infty}^{\infty}\sum_{l=2}^{k}\frac{\Upsilon_{l\rho}^{(1)}\left[2|\mu_{l,r}|+(\omega_0^2\rho^2 c)\right]+2\Delta_{l\rho}^{(1)}\left[\omega_m+\mu_{l,i}\right]}{\left(|\mu_{l,r}|+(0.5\omega_0^2\rho^2 c)\right)^2+\left(\omega_m+\mu_{l,i}\right)^2}$$

which implicitly contains S-OSC spectrum as the trivial special case $k=1$ (i.e., free-running oscillator/no coupling). The various components of the above equation are explained in Section 6; however, the important point to note here is that it depends only on components which derive directly from the eigenvalues/eigenvectors of the Monodromy matrix (see Section 2.3); that is, the Floquet decomposition. The Monodromy matrix is calculated from the Jacobian variational equations which derives directly from the system ODE and corresponding PSS. As such, the model proposed herein is completely generalized and can be applied to all possible coupled configurations.

## 2 | BASIC BACKGROUND THEORY

Our model domain is the $n$-dimensional state-space $\mathcal{X}\subset\mathbb{R}^n$ with standard Euclidian coordinates $x=(x_1,x_2,\ldots,x_n)^\top\in\mathbb{R}^n$, that is, the *state-vector*, where throughout, symbols, $\top$ and $\dagger$, represent the transpose and Hermitian (transpose + complex conjugate) operators, respectively. The dynamics on $\mathcal{X}$ is governed by an $n$-dimensional SDE

$$\dot{x}=f(x)+b(x)\xi(t) \tag{1}$$

where $f:\mathbb{R}^n\to\mathbb{R}^n$ is the autonomous vector-field, $b:\mathbb{R}^n\to\mathbb{R}^{n\times p}$ is the so-called *noise-modulation matrix* and $\xi(t):\mathbb{R}\to\mathbb{R}^p$ is a $p$-dimensional vector of uncorrelated, white, Gaussian noise sources with zero mean and unit power, with all noise-power information being contained in $b$. The model assumes a *weak-noise* scenario $\|b(x(t))\xi(t)\|\ll 1$ for all $t$ which describes all physical systems operating at or around room temperature. The solution produced by the corresponding deterministic ODE $\dot{x}=f(x)$ (i.e., no noise) is written as $x(t)=\psi_t(x_0)$ where $x_0\in\mathbb{R}^n$ is the initial state of the system at time $t=0$ with $\psi_t$ known as the *flow*. Herein, we consider the synchronized state of an ensemble of coupled oscillators. In this scenario, the asymptotic dynamics is governed by one-dimensional invariant, NH set, $\gamma$, known as the *limit-cycle*. This is a $\omega$-limit set which implies that all orbits approach this set asymptotically with time. The PSS solution $x_s(t+T_0)=x_s(T_0)$ is a $T_0$-periodic orbit, corresponding to an initial condition in $\gamma$; that is, $x_s(t)=\psi_t(x_0)$ with $x_0\in\gamma$.

### 2.1 | The C-OSC state equations

We consider an ensemble of $k$ autonomous oscillator units coupled together in some manner; a so-called $k$-order ensemble. Let $m_i$ be the state dimension of the $i$th oscillator unit in the ensemble with $\sum m_i=n$. The $n$-dimensional state-vector $x$ and vector-field $f$ in Equation (1) are then partitioned as $x^{(i)}(t):\mathbb{R}\to\mathbb{R}^{m_i}$ and $f^{[i]}:\mathbb{R}^n\to\mathbb{R}^{m_i}$ where $f^{[i]}(x)=g^{[i]}(x^{(i)})+w^{[i]}(x,\lambda)\ i=1,2,\ldots,k$ with $g^{[i]}:\mathbb{R}^{m_i}\to\mathbb{R}^{m_i}$ governing the internal oscillator dynamics, whereas $w^{[i]}(x,\lambda)$:

$\mathbb{R}^n \times \mathbb{R}^c \to \mathbb{R}^{m_i}$ holds the coupling contribution depending on $c$ parameters combined into the vector $\lambda \in \mathbb{R}^c$. These coupling parameters control the strength of the coupling such that

$$\lim_{\lambda \to \mathbf{0}} w^{[i]}(x,\lambda) = 0,\ i = 1,2,...,k \tag{2}$$

where $\mathbf{0} = (0,0,...,0) \in \mathbb{R}^c$ is the $c$-dimensional zero-vector. Let $\lambda_0 \in \mathbb{R}^c$ represent some given unit-vector in the coupling parameter space $\|\lambda_0\| = 1$. The *global coupling* strength parameter $\epsilon$ is then introduced through $\lambda = \epsilon\lambda_0$. From Equation (2), $\lim_{\lambda\to\mathbf{0}} w^{[i]}(x,\lambda) = \lim_{\epsilon\to 0} w^{[i]}(x,\epsilon\lambda_0) = 0$ which implies $\lim_{\epsilon\to 0} f^{[i]}(x) = g^{[i]}(x^{(i)})$ describing C-OSC *uncoupled* scenario with $k$ free-running oscillator units. The global coupling parameter, $\epsilon$, thus controls the transition (uncoupled $\to_\epsilon$ coupled) which, given the proper parameter settings, leads to the transition from C-OSC uncoupled (free-running) dynamics to a potential synchronized state.

## 2.2 | The $\gamma$-tangent bundle

The limit-cycle *tangent-space* $\mathsf{T}_\eta\mathbb{R}^n$ is an affine (translated) linear vector-space with origin at the point $x_s(\eta) \in \gamma$ (i.e., simply the standard $\mathbb{R}^n$ with origin translated to $x_s(\eta)$). The corresponding *tangent-bundle* is then constructed as the disjoint union of the individual tangent spaces based on the steady-state solution $x_s(t) \in \gamma$

$$\mathsf{T}_\gamma\mathbb{R}^n = \bigcup_{\eta\,\in\,[0;\,T_0]} \mathsf{T}_\eta\mathbb{R}^n \tag{3}$$

with $x_s$ then referred to as the bundle *base-space*. As $\gamma$ is assumed hyperbolic, it follows[5,6,8,31] that there exists a unique set of $n$ complex Floquet vectors $u_i(t) : \mathbb{R} \to \mathbb{C}^n$ and dual (co-variant) complex Floquet vectors $v_i(t) : \mathbb{R} \to \mathbb{C}^n$ directly associated to this PSS. The $T_0$-periodic vectors/dual-vectors in $\{u_i(t)\}$ and $\{v_i(t)\}$ form complete sets and the $\gamma$-tangent bundle (3) can thus be written

$$\mathsf{T}_\gamma\mathbb{R}^n = \text{span}\{u_1(\eta), u_2(\eta), ...u_n(\eta)\} \tag{4}$$

where throughout we assume $\eta \in [0;\, T_0]$. The corresponding dual cotangent-bundle, $\mathsf{T}^*_\gamma\mathbb{R}^n$, is expressed as[8]

$$\mathsf{T}^*_\gamma\mathbb{R}^n = \text{span}\{v_1(\eta), v_2(\eta), ...v_n(\eta)\} \tag{5}$$

As the dynamics discussed here describes physical systems with a purely real state, it follows that all vectors/dual-vectors with nonzero complex parts must be paired with complex-conjugated twin objects, that is, $u_i = u^*_{i+1}$.

## 2.3 | The Floquet decomposition of the LR

We consider the PSS, $x_s(t)$, perturbed by a weak signal $\zeta(t) : \mathbb{R} \to \mathbb{R}^n$, $\|\zeta\|^2 \ll 1$. The expansion around $x_s$ is then written $x(t) = x_s(t) + x_{\text{LR}}(t) + \mathcal{O}(\|\zeta\|^2)$ where $x_{\text{LR}} : \mathbb{R} \to \mathbb{R}^n$ is first-order in $\zeta$ and hence referred to as the *linear response* (LR). The LR follows as the solution to the Jacobi variational equation $d(x_{\text{LR}}(t))/dt - J(t)x_{\text{LR}}(t) = 0$, where $J : \mathbb{R} \to \mathbb{R}^{n\times n}$ is the Jacobian of the vector-field $f$ defined in Equation (1) evaluated on $x_s(t) \in \gamma$. The corresponding fundamental matrix (F-MATRIX) solution of this linear time-varying (LTV) Jacobi equation is written $d\psi(t,s) : \mathsf{T}_s\mathbb{R}^n \to \mathsf{T}_t\mathbb{R}^n$ with $t,s \in \mathbb{R}$. With this notation, the LR solution, in response to the weak perturbation source $\zeta(t)$, is written

$$x_{\text{LR}}(t) = d\psi(t,s)\delta x_0 + \int_s^t d\psi(t,\eta)\zeta(\eta)d\eta \tag{6}$$

where $x_{\text{LR}}(s) = \delta x_0$ represents an initial condition. Herein, we will often use the simplified, but fully equivalent, notation $d\psi_q = d\psi(t,s) = d\psi(t-s,0) = d\psi(q,0)$ which holds for autonomous flows. For a hyperbolic stable limit-cycle, $\gamma$, the F-MATRIX always has a unique Floquet decomposition[5,6,8]

$$d\psi(t,s) = \sum_{j=1}^{n} \exp(\mu_j(t-s)) u_j(t) v_j^{\top}(s) \tag{7}$$

where the sets $\{u_i(t), v_i(t)\}$ were introduced above in connection with Equations (4)–(5) and $\mu_i$ are the $n$ complex characteristic Floquet exponents where $\Re\{\mu_i\} \leq 0$ (real part) must hold to ensure stability of the PSS solution.[31] The special F-MATRIX $\Psi = d\psi(T_0,0) = d\psi_{T_0}$ is known as the *Monodromy matrix* and from Equation (7) $\Psi = \sum_{j=1}^{n} \lambda_i u_j(T_0) v_j^{\top}(0)$, where $\lambda_i = \exp(\mu_j T_0)$ are known as the Floquet *characteristic multipliers*. Herein, the set $\{u_i, v_i, \lambda_i, \mu_i\}$, or individual members of this 4-tuple, will be referred to as the *i*th *(Floquet) mode*. The Floquet vectors and dual vectors of different modes are mutually bi-orthogonal $v_i^{\top}(t) u_j(t) = \delta_{ij}$ where $\delta_{ij}$ is the Kroenecker delta-function. As the set $\{u_i(t)\}$ is complete, we can write any state-vector $\zeta(t) : \mathbb{R} \to \mathbb{R}^n$ on the form $\zeta(t) = a_1(t)u_1(t) + a_2(t)u_2(t) + \ldots + a_n(t)u_n(t)$ where $a_i(t) : \mathbb{R} \to \mathbb{C}$ are $n$ expansion coefficient-functions. Using the bi-orthogonality condition, it then follows that $v_i^{\top}(t)\zeta(t) = a_i(t)$ and the dual vector $v_i$ hence picks out the component of $\zeta$ proportional to $u_i$. The dynamics tangential to the limit-cycle $\gamma$ is, by definition, neutrally stable. A special Floquet mode, with characteristic exponent equal to zero, is then known to always exist.[5,6,26] This special mode, $\{u_1, v_1, \lambda_1 = 1, \mu_1 = 0\}$, will be referred to here as the *$\gamma$-phase-mode*. This mode is furthermore characterized by the fact that $u_1(t)$ is proportional to $\dot{x}_s$[5,6,8] which implies that we can fix

$$u_1(t) = \dot{x}_s(t) \tag{8}$$

## 2.4 | Basic invariant manifold theory: C-OSC synchronized dynamics

Consider a $q$-dimensional submanifold $\mathcal{M}$, with $1 < q \leq \lfloor n/2 \rfloor$, embedded in the C-OSC state-space $\mathcal{X} \subset \mathbb{R}^n$, which is *invariant* under the flow, that is, $\psi_t(\mathcal{M}) \subset \mathcal{M}$ for all $t$. The C-OSC synchronized state dynamics involves a single $\omega$-limit set, $\gamma$, also known as the limit-cycle.

**Lemma 2.1.** The limit-cycle, $\gamma$, is embedded (i.e., has coordinate description) in $\mathcal{M}$ and is hence a regular submanifold of this space (see Figure 1A).

*Proof.* As it is a limit-set, $\gamma$ is, by definition, invariant under the flow $\psi_t(\gamma) \subset \gamma$. Hence, both $\mathcal{M}$ and $\gamma$ are invariant under the flow. Since the basin of attraction of both sets is assumed to be the entire state-space, $\mathcal{X}$, this then directly implies $\gamma \subset \mathcal{M}$. The set $\gamma$ is, by definition, an embedded submanifold in $\mathcal{X}$. Let $\beta$ and $\iota$ be the smooth inclusions of $\gamma$ and $\mathcal{M}$, respectively, in $\mathcal{X}$. Then, $\iota^{-1} \circ \beta : \gamma \mapsto \mathcal{M}$ is a smooth embedding of $\gamma$ in $\mathcal{M}$.

The $q$-dimensional tangent space to $\mathcal{M}$ at a point, $x \in \mathcal{M}$, is written $\mathsf{T}_x\mathcal{M}$. From Lemma 2.1, $x_s(t) \in \gamma \subset \mathcal{M}$, and we define $\mathsf{T}_\eta\mathcal{M}$ to represent the tangent space of $\mathcal{M}$ at the point $x_s(\eta)$. The corresponding $q$-dimensional bundle $\mathsf{T}_\gamma\mathcal{M}$ is then defined as the disjoint union of these vector-spaces

$$\mathsf{T}_\gamma\mathcal{M} = \bigcup_{\eta \in [0; T_0[} \mathsf{T}_\eta\mathcal{M} \tag{9}$$

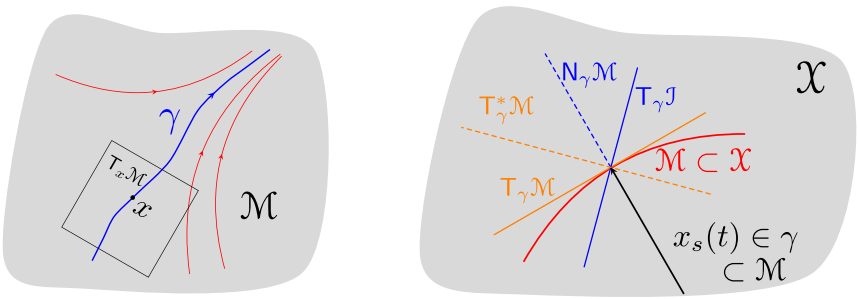


**(A)** $\gamma \subset \mathcal{M}$. **(B)** $\mathsf{T}_\gamma\mathbb{R}^n$ and $\mathsf{T}_\gamma^*\mathbb{R}^n$.

**FIGURE 1** (A) The limit-cycle $\gamma$ (blue orbit) is embedded in $\mathcal{M}$. All orbits on, and off, $\mathcal{M}$ approach this one-dimensional (1-D) set asymptotically with time (red orbits). The tangent space to $\mathcal{M}$ at a point $x \in \mathcal{M}$, $\mathsf{T}_x\mathcal{M}$, is an affine copy of $\mathbb{R}^q$. (B) The $\gamma$-tangent bundle is decomposed as $\mathsf{T}_\gamma\mathbb{R}^n = \mathsf{T}_\gamma\mathcal{M} \bigoplus \mathsf{T}_\gamma\mathcal{I}$, whereas the dual tangent-bundle is written $\mathsf{T}_\gamma^*\mathbb{R}^n = \mathsf{T}_\gamma^*\mathcal{M} \bigoplus \mathsf{N}_\gamma\mathcal{M}$ (broken line). These bundles have the 1-D base-space $\gamma \subset \mathcal{M} \subset \mathcal{X}$ traced out by the steady-state solution $x_s(t)$ [Colour figure can be viewed at wileyonlinelibrary.com]

**Lemma 2.2.** The tangent-bundle $\mathsf{T}_\gamma\mathcal{M}$ is spanned by $q$ Floquet vectors

$$\mathsf{T}_\gamma\mathcal{M} = \text{span}\{u_{i_1}(\eta), u_{i_2}(\eta), ..., u_{i_q}(\eta)\} \tag{10}$$

*Proof.* The tangent bundle of an invariant manifold is, by definition, invariant under the LR flow $d\psi_t(\mathsf{T}\mathcal{M}) \subset \mathsf{T}\mathcal{M}$. Here, $\mathsf{T}_\gamma\mathcal{M}$ denotes the sub-bundle of $\mathsf{T}\mathcal{M}$ over the base-space $\gamma \subset \mathcal{M}$. Since, from Lemma 2.1, $\gamma$ is itself an invariant manifold embedded in $\mathcal{M}$ it follows, by definition, that $d\psi_t(\mathsf{T}_\gamma\mathcal{M}) \subset \mathsf{T}_\gamma\mathcal{M}$. As the sub-bundle is invariant, the result follows directly from Lemma A.2 in Appendix A.

As $\mathsf{T}_\gamma\mathcal{M}$ is the tangent bundle of $\mathcal{M}$ with base-space $\gamma \in \mathcal{M}$, it follows that $u_1(t) = \dot{x}_s(t)$ (see Equation 8) must be an element of the bundle in Equation (10). With the exception of the special phase-mode $u_1(t)$, the numbering of the Floquet modes is completely arbitrary, and the remaining $q-1$ modes in Equation (10) are then simply assigned indices 2 to $q$. Given this choice of numbering, the full $\gamma$ tangent-bundle, $\mathsf{T}_\gamma\mathbb{R}^n$, defined in Equation (4) of Section 2.2, is then decomposed as

$$\mathsf{T}_\gamma\mathbb{R}^n = \mathsf{T}_\gamma\mathcal{M} \bigoplus \mathsf{T}_\gamma\mathcal{I} \tag{11}$$

with

$$\begin{aligned} \mathsf{T}_\gamma\mathcal{M} &= \text{span}\{u_1(\eta), u_2(\eta), ..., u_q(\eta)\} \\ \mathsf{T}_\gamma\mathcal{I} &= \text{span}\{u_{q+1}(\eta), u_{q+2}(\eta), ..., u_n(\eta)\} \end{aligned} \tag{12}$$

where $\mathsf{T}_\gamma\mathcal{M}$ is the $q$-dimensional sub-bundle tangent to $\mathcal{M}$, whereas $\mathsf{T}_\gamma\mathcal{I}$ is the $(n-q)$-dimensional sub-bundle spanning directions traverse to $\mathcal{M}$. The dual cotangent space defined in Equation (5) of Section (2.2) can then also be decomposed

$$\mathsf{T}^*_\gamma\mathbb{R}^n = \mathsf{T}^*_\gamma\mathcal{M} \bigoplus \mathsf{N}_\gamma\mathcal{M} \tag{13}$$

with

$$\begin{aligned} \mathsf{T}^*_\gamma\mathcal{M} &= \text{span}\{v_1(\eta), v_2(\eta), ..., v_q(\eta)\} \\ \mathsf{N}_\gamma\mathcal{M} &= \text{span}\{v_{q+1}(\eta), v_{q+2}(\eta), ..., v_n(\eta)\} \end{aligned} \tag{14}$$

where $\mathsf{T}^*_\gamma\mathcal{M}$ and $\mathsf{N}_\gamma\mathcal{M}$ are the dual sub-bundles of $\mathsf{T}_\gamma\mathcal{M}$ and $\mathsf{T}_\gamma\mathcal{I}$, respectively. The above discussion is illustrated schematically in Figure 1B.

## 3 | THE C-OSC PHASE-MANIFOLD $\mathcal{P}$

The C-OSC system is uncoupled for $\epsilon = 0$, where $\epsilon \in \mathbb{R}$ is the scalar global coupling parameter (see Section 2.1). The uncoupled state directly implies the following $k$-dimensional invariant manifold

$$\mathcal{P}_0 = x_s^{(1)}(\eta_1) \times x_s^{(2)}(\eta_2) \times ... \times x_s^{(k)}(\eta_k) \tag{15}$$

where $x_s^{(i)}(t) : \mathbb{R} \to \mathbb{R}^{m_i}$ denotes steady-state vector of the $i$th oscillator unit (free-running) in the ensemble and $\eta = [\eta_1, \eta_2, ..., \eta_k] \in \mathbb{R}^k$ are the manifold coordinates.

**Lemma 3.1.** The manifold $\mathcal{P}_0$ is a normally hyperbolic invariant manifold (NHIM), smoothly embedded in the state-space $\mathcal{X}$ and diffeomorphic (i.e., smoothly related) to the $k$-torus $\mathbb{T}^k = \mathbb{S} \times \mathbb{S} \times ... \times \mathbb{S}$ ($k$ times).

*Proof.* See Appendix B.

At this point, the coupling is increased (i.e., $\epsilon \uparrow$). We are interested in understanding whether the manifold, $\mathcal{P}_0$, in Equation (15) will survive this parameter perturbation. In other words, we seek to understand if $\mathcal{P}_0$ *persists* the coupling perturbation.

**Lemma 3.2.** There exists an open range, $\epsilon \in [0; \epsilon_f[$ such that $\mathcal{P}_0$ in Equation (15) persists. The resulting deformation (i.e., transformed manifold), $\mathcal{P}$, is an NHIM smoothly embedded $\mathcal{X}$ diffeomorhic to the $k$-torus $\mathbb{T}^k$.

*Proof.* See Appendix B.

In the following, we shall refer to this NHIM, $\mathcal{P} \subset \mathcal{X}$, and its un-coupled counterpart $\mathcal{P}_0 = \lim_{\epsilon \to 0} \mathcal{P}$, as the C-OSC *phase-manifold*. Note that the above result is fully independent of the specific direction in parameter space, as prescribed by the unit coupling vector $\lambda_0 \in \mathbb{R}^c$ (see Section 2.1), chosen for the coupling; it only relies on $\mathcal{P}_0$ initially being NHIM. Up until this point, we have not mentioned synchronization. Thus, increasing the coupling $\epsilon \uparrow$ may, or may not, have resulted in a synchronized state of the ensemble with Lemmas 3.1–3.2 above being independent of this issue. However, as the topic of this paper concerns synchronized ensembles, we henceforth implicitly assume that coupling is arranged in such a manner that synchronization is achieved. The C-OSC system being assumed synchronized, the dynamics are thus characterized by the presence of a one-dimensional limit-cycle $\gamma$.

**Lemma 3.3.** The C-OSC limit-cycle, $\gamma$, is embedded in the phase-manifold, $\mathcal{P}$, and the sub-bundle $\mathsf{T}_\gamma \mathcal{P}$ is spanned by $k$ unique Floquet modes

$$\mathsf{T}_\gamma \mathcal{P} = \text{span}\{u_1(\eta), u_2(\eta), ..., u_k(\eta)\} \tag{16}$$

*Proof.* Follows directly from Lemmas 2.1–2.2 and Equation (12), from Section 2.4, with $q = k$.

The $k$ modes in Equation (16) are referred to as the *phase-modes* in the discussion below. The following result will prove useful

**Lemma 3.4.** The Floquet multipliers $\{\lambda_i\}_{i=1}^k$, corresponding to the $k$ phase-modes in Equation (16), each obey the limit condition $\lim_{\epsilon \to 0} \lambda_i = 1.0$.

*Proof.* See Appendix B.

## 4 | A C-OSC AMPLITUDE-PHASE REPRESENTATION

The C-OSC state is described in terms of the Euclidian coordinate state-vector $x = (x_1, x_2, ..., x_n)^\top \in \mathbb{R}^n$. In this section, we seek to introduce an alternative *amplitude-phase coordinate representation* in some open subset $\mathcal{S} \subset \mathcal{X}$. Importantly, $\mathcal{S}$ is assumed to include the NHIM phase-manifold $\mathcal{P}$. In other words, the phase-manifold is embedded (has coordinate description) in this space $\mathcal{P} \subset \mathcal{S}$. Thus, at each point $p \in \mathcal{S}$, an alternative coordinate representation is assumed to exist

$$z = \beta(x) = (z_1, z_2, ..., z_n) = (\phi, y) = (\phi_1, \phi_2, ..., \phi_q, y_1, y_2, ..., y_{n-q}) \tag{17}$$

where $z \in \mathbb{R}^n$ are referred to as the *amplitude-phase coordinates* with $\phi \in \mathbb{R}^q$ and $y \in \mathbb{R}^{n-q}$ being the phase and amplitude subcoordinate vectors, respectively. Given two smooth sets of coordinates, $x$ and $z$, parameterizing $\mathcal{S}$, it follows, by

definition, that a smooth map (diffeomorphism) $\beta : \mathbb{R}^n \to \mathbb{R}^n$ exists transforming between these two representations[32,33] $\beta : x \mapsto z = (\phi, y)$ as illustrated schematically in Figure 2. The phase coordinates $\phi \in \mathbb{R}^q$ are, by definition, periodic coordinates.

**Definition 4.1 A definition of periodic coordinates.** Consider the point $p = \beta^{-1}(z) = \beta^{-1}(\phi, y)$ on manifold $\mathcal{S}$. Now advance the $i$ th phase coordinate $\phi_i \to \phi_i + \sigma_i$ leading to the new phase vector $\tilde{\phi} = \phi + j\sigma_i \hat{e}_i \in \mathbb{R}^q$ where $\hat{e}_i = (0, 0, ...0, 1, 0, \cdot, 0) \in \mathbb{R}^q$ is the Euclidian unit vector (all zero except $i$ th component) and $j \in \mathbb{Z}$ is some integer. This coordinate transformation hence produces the new point $\tilde{p} = \beta^{-1}(\tilde{z}) = \beta^{-1}(\tilde{\phi}, y)$. Then, coordinate $\phi_i$ is said to be periodic, with period $\sigma_i$, if $p = \tilde{p}$ holds on $\mathcal{S}$.

For a $k$-order C-OSC system ($k$ coupled oscillators), the number of phase variables, that is, the phase order, is exactly $q = k$

**Lemma 4.1.** For a $k$-order ensemble, $\mathcal{S}$ is parameterized by exactly $k$ periodic coordinates (phase coordinates) $\phi = (\phi_1, \phi_2, ..., \phi_k) \in \mathbb{R}^k$ and these parameterize the phase-manifold $\mathcal{P}$. The embedded one-dimensional limit-cycle set $\gamma \subset \mathcal{P}$ is parameterized by the single-phase coordinate $\phi_1$.

*Proof.* See Appendix B.

The order of this amplitude-phase decomposition, $\phi \in \mathbb{R}^k$ and $y \in \mathbb{R}^{n-k}$, thus uniquely follow from the dimension of the $k$-dimensional phase-manifold $\mathcal{P}$ which in-turn follows from the order of the coupled C-OSC ensemble (i.e., a $k$-order ensemble, see Section 2). The following remark follows directly from the above lemma.

*Remark* 4.1. In $z = (\phi, y)$-coordinates, the phase-manifold $\mathcal{P}$, for a $k$-order ensemble, is represented by the $k$-slice $y = \mathbf{0}$; that is, parameterized by the $k$ coordinates $\phi = (\phi_1, \phi_2, ..., \phi_k) \in \mathbb{R}^k$ with $y = \mathbf{0} = (0, 0, ..., 0) \in \mathbb{R}^{n-k}$, whereas $\gamma$ corresponds to the $z$-coordinate 1-slice $\{\phi_{k>1}, y\} = \mathbf{0} \in \mathbb{R}^{n-1}$.

The coordinate vector corresponding to a coordinate $w$ is traditionally written $\partial/\partial w$ to emphasize the relation between coordinate vectors and directional derivatives. Herein, we shall use simplified notation $\partial_{\boldsymbol{w}}$ to convey the same information. The coordinate vectors following from the $z$-coordinate system, developed above, are then written $\partial_{\boldsymbol{z}} = (\partial_{\boldsymbol{\phi}}, \partial_{\boldsymbol{y}})$. These vectors are then mapped by the Jacobian $d\beta^{-1}$ of the coordinate transformation map $\beta^{-1} : z \mapsto x$ (see Equation 17) to produce the $x$-coordinate representation of these vectors $\partial x/\partial z_i = (\partial x(t)/\partial \phi_i), (\partial x/\partial y_i)$; also

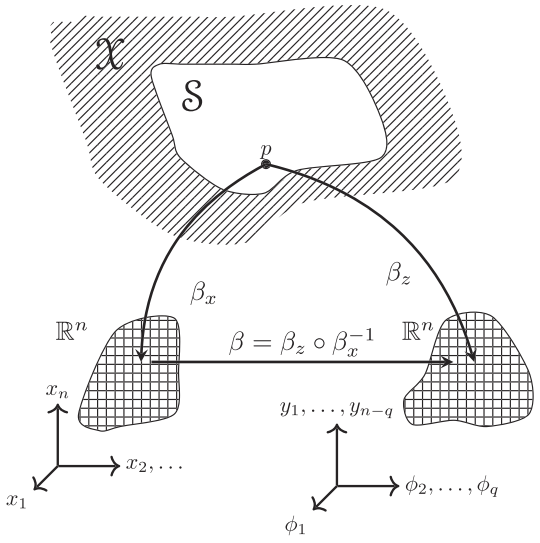


**FIGURE 2** The subset $\mathcal{S} \subset \mathcal{X}$ is parameterized by both the Euclidian $x$-coordinates with coordinate map $\beta_x : \mathcal{X} \to \mathbb{R}^n$ as well as the (amplitude-phase) $z$-coordinates with coordinate map $\beta_z : \mathcal{X} \to \mathbb{R}^n$. A point $p \in \mathcal{S}$ hence has smooth representations in both coordinate systems with $\beta = \beta_z \circ \beta_x^{-1}$ being the smooth coordinate transformation

known as the push-forward vectors.[32,33] The tangent space at a point $p \in \mathcal{P}$ is then decomposed as $\mathsf{T}_p\mathbb{R}^n = \mathsf{T}_p\mathcal{P} \bigoplus \mathsf{T}_p\mathcal{I}$, where $\mathsf{T}_p\mathcal{P}$ is the $k$-dimensional tangent space to $\mathcal{P}$ and $\mathsf{T}_p\mathcal{I}$ represents directions traverse to $\mathcal{P}$ (see discussion in Sections 2.4 and 3). From Lemma 4.1, $\mathcal{P}$ is parameterized by the $k$ coordinates $\phi \in \mathbb{R}^k$. By definition, the corresponding coordinate vectors at a point $p \in \mathcal{P}$, then span the tangent space of this manifold at this same point.[32] From this description, it follows that we can write the phase-manifold tangent bundle $\mathsf{T}_\gamma\mathcal{P}$, introduced in Section 3 above (see Lemma 3.3), on the form

$$\mathsf{T}_\gamma\mathcal{P} = \text{span}\{\varrho_1(\eta), \varrho_2(\eta), ..., \varrho_k(\eta)\} \tag{18}$$

where

$$\varrho_i(t) = (\partial x(t)/\partial \phi_i)|_{x(t)=x_s(t)}\,, i = 1,2,...k \tag{19}$$

## 5 | THE C-OSC LR PHASE EQUATIONS

The previous section introduced the coordinates $z = (\phi, y)$ specifying C-OSC amplitude and phase coordinates on the open set $\mathcal{S} \subset \mathcal{X}$ in which the phase manifold is embedded $\mathcal{P} \subset \mathcal{S}$. Using the results from Lemma 4.1 and Remark 4.1, as well as the shorthand $x(z) = x(\phi, y) = x(\phi, y = \mathbf{0}) = x(\phi)$, orbits on $\mathcal{P}$ are written

$$x(t) \underset{x \in \mathcal{P}}{=} x(\phi_1(t), \phi_2(t), ..., \phi_k(t)) = x(\{\phi_j(t)\}), j = 1,2,...,k \tag{20}$$

From the C-OSC SDE in Equation (1), the system is driven by the weak-noise source-vector $\zeta(x,t) = b(x(t))\xi(t) : \mathbb{R}^n \times \mathbb{R} \to \mathbb{R}^n$. The response of the phase variables $\{\phi_j(t)\}$, to this stochastic perturbation, is then written

$$\phi_j(t) = \underbrace{\hat{\phi}_j(t)}_{\text{deterministic}} + \underbrace{\delta\phi_j(t)}_{\text{stochastic}} \tag{21}$$

where the $k$ functions $\{\delta\phi_j(t)\}$ represent the stochastic response, away from the deterministic orbit. We seek to develop the phase-response around the steady-state solution $x_s(t) \in \gamma$. From Lemma 4.1, it follows that $x_s(t) = x(\hat{\phi}_1(t)) \in \gamma$ which implies that for the PSS on $\gamma \in \mathcal{P}$, that is, $x_s(t)$, we have

$$\hat{\phi}_j(t) = \begin{cases} t & \text{for} j = 1 \\ 0 & \text{otherwise} \end{cases} \tag{22}$$

Inserting Equation (21) into Equation (20) and using Equation (22) gives

$$\begin{aligned} x\Big(\{\phi_j(t)\}\Big) &= x\Big(\{\hat{\phi}_j(t) + \delta\phi_j(t)\}\Big) \\ = x\big(\hat{\phi}_1(t) + \delta\phi_1(t), \hat{\phi}_2(t) + \delta\phi_2(t), ..., \hat{\phi}_k(t) + \delta\phi_k(t)\big) &= x(t + \delta\phi_1(t), \delta\phi_2(t), \delta\phi_3(t), ..., \delta\phi_k(t)) \end{aligned} \tag{23}$$

From the above discussion, it follows that the coordinates $\{\phi_j(t)\}_{j\geq 2}$ describe directions tangent to $\mathcal{P}$ but traverse to the embedded limit-cycle $\gamma$. Since $\gamma$ is a $\omega$-limit-set all orbits approach, this set asymptotically with time. A response excited in a direction traverse to $\gamma$ is hence contracted and thus cannot grow unimpeded. This response is hence always bounded by the size of the stochastic excitation $\zeta$, and we can thus write

$$\big\langle (\delta\phi_j(t))^2 \big\rangle = \mathcal{O}\big(\big\langle \|\zeta(t)\|^2 \big\rangle\big) \ll 1\,, \text{for} j \geq 2 \tag{24}$$

where $\zeta(t) = b(x_s(t))\xi(t)$. In contrast, the dynamics along $\gamma$ are neutrally stable (no contraction) which implies that the variance/power of the stochastic phase-mode, $\delta\phi_1$, grows w/o bound. In order to emphasize this issue, we relabel this special coordinate

$$\alpha(t) := \delta\phi_1(t) \tag{25}$$

Equation (24) implies that the stochastic response of the phase coordinates $\{\phi_j\}_{j>1}$, to a good approximation, can be moved outside the argument in Equation (23). Taylor expanding Equation (23) *w.r.t.* the bounded coordinates $\phi_{(j>1)}$, around the PSS (i.e., $\phi_j(t)=\hat{\phi}_j(t)$), gives

$$x(\{\phi_i(t)\})=x_s(t+\alpha(t))+\sum_{i=2}^{k}\varrho_i(t+\alpha(t))\delta\phi_i(t+\alpha(t))+\mathcal{O}\left(\left\langle\|\zeta(t)\|^2\right\rangle\right) \tag{26}$$

where $\varrho_i(t):\mathbb{R}\to\mathbb{R}^n$ are defined in Equation (19). Here, Equation (26) uses the shorthand $x_s(t+\alpha(t))\equiv x(\phi_1(t),\widehat{\phi_2}(t),\widehat{\phi_3}(t),\ldots,\widehat{\phi_k}(t))=x(\phi_1(t),0,0,\ldots,0)=x(t+\alpha(t),0,0,\ldots,0)$ (see Equations 22 and 25) and similarly for $\varrho_i(t+\alpha(t))$. This notation represents the fact that $x_s(t)\in\gamma$ is parameterized by the single-phase coordinate $\phi_1$, with $\hat{\phi}_{(j>1)}=0$ (deterministic component) as follows from Equation (22). The theory developed in this and the two previous sections is now used to develop the following model of C-OSC phase-noise response

**Lemma 5.1.** The stochastic phase dynamics of a general synchronized C-OSC, $k$-order ensemble, system, perturbed by weak noise, around the asymptotic limit-cycle PSS $x_s(t)\in\gamma$, is governed by the $k$ unique Floquet modes $\{u_1, u_2, \ldots, u_k\}$. The linear (first-order) expansion, w.r.t. these phase coordinates $\{\phi_j\}$, is then written

$$x_{\mathrm{LR}}\left(\{\phi_j(t)\}\right)=x_s(t+\alpha(t))+\sum_{j=2}^{k}u_j(t+\alpha(t))\delta\phi_j(t+\alpha(t)) \tag{27}$$

The LR phase coordinate functions $(\alpha,\{\delta\phi_j\})$ are characterized by the stochastic integrals

$$\alpha(t+\tau)-\alpha(t)=\int_{t}^{t+\tau}\nu_1^{\top}(\eta)b(x_s(\eta))\xi(q)d\eta \tag{28}$$

and, assuming $\delta\phi_j(-\infty)=0$,

$$\delta\phi_j(t+\alpha(t))=\int_{-\infty}^{t+\alpha(t)}\exp(-\mu_j(\eta-[t+\alpha(t)]))\nu_j^{\top}(\eta)b(x_s(\eta))\xi(\eta)d\eta,\ j=2,3,\ldots,k \tag{29}$$

*Proof.* From Equation (16), in Lemma 3.3 and Equation (18), in Section 4, both sets $\{u_i(\eta)\}_{i=1}^{k}$ and $\{\varrho_i(\eta)\}_{i=1}^{k}$ span the phase-manifold bundle $\mathsf{T}_\gamma\mathcal{P}$, and we can hence find a parametrization such that $\varrho_i(t)=(\partial x(t)/\partial\phi_i)|_{x(t)=x_s(t)}=u_i(t)$ and Equation (27) follows from Equation (26) by ignoring higher order terms. Equations (28)–(29) then follow directly from Equation (6) in Section 2.3 with the weak noise drive $\zeta(t)=b(x_s(t))\xi(\tau)$ defined in connection with Equation (1).

## 6 | THE C-OSC SINGLE-SIDED PHASE-NOISE SPECTRUM

The C-OSC cross power-density phase spectrum, $S(\omega):\mathbb{R}\to\mathbb{C}^{n\times n}$, is defined as $\mathfrak{F}(C_s(\tau))$ where $\mathfrak{F}(\bullet)$ is the Fourier transform operator and $C_s(\tau):\mathbb{R}\to\mathbb{R}^{n\times n}$ is the LR C-OSC phase cross-correlation matrix

$$C_s(\tau)=\lim_{t\to\infty}\left\langle x_{\mathrm{LR}}(\{\phi_j(t)\})x_{\mathrm{LR}}^{\top}(\{\phi_j(t+\tau)\})\right\rangle \tag{30}$$

where $x_{\mathrm{LR}}(\{\phi_j(t)\})$ refers to the linear (first-order) response. An expression for the C-OSC LR was derived in previous section (see Lemma 5.1) and inserting Equation (27) into Equation (30) gives

$$C_s(\tau)=\lim_{t\to\infty}\left\langle\left(x_s(t+\alpha(t))+\sum_{j=2}^{k}w_j(t+\alpha(t))\right)\left(x_s(t+\tau+\alpha(t+\tau))+\sum_{j=2}^{k}w_j(t+\tau+\alpha(t+\tau))\right)^{\dagger}\right\rangle \tag{31}$$

where we have introduced the vector-functions $w_j : \mathbb{R} \to \mathbb{C}^n$ as

$$w_j(s) = u_j(s)\delta\phi_j(s), j = 2,3,...,k \tag{32}$$

The matrix in Equation (30) is now expanded as

$$C_s(\tau) = \sum_{\nu} C_s^{(\nu)}(\tau)\exp(-j\nu\omega_0\tau). \tag{33}$$

where $C_s^{(\nu)} : \mathbb{R} \to \mathbb{R}^{n\times n}$ is the $\nu$th harmonic envelope of $C_s$. Fourier transforming this expansion then gives the following expression for the spectrum $S(\omega) = \sum_{\nu=-\infty}^{\infty}\int_{-\infty}^{\infty} S^{(\nu)}(q)\delta([\omega-\nu\omega_0]-q)dq = \sum_{\nu=-\infty}^{\infty} S^{(\nu)}\left(\omega_m^{(\nu)}\right)$, where $S^{(\nu)}(\omega) = \mathfrak{F}(C_s^{(\nu)}(\tau)) : \mathbb{R} \to \mathbb{C}^{n\times n}$ is the $\nu$th envelope spectrum and $\omega_m^{(\nu)} = \omega - \nu\omega_0$ ($\omega_0 = 2\pi/T_0$) is the *offset-frequency* around the $\nu$th harmonic. Let $x_{s,q}(t) : \mathbb{R} \to \mathbb{R}$ be the $q$th component of the steady-state vector $x_s(t) = (x_{s,1}(t), x_{s,2}(t), ..., x_{s,n}(t))^{\top} \in \mathbb{R}^n$. The C-OSC phase auto-correlation for this variable, $\langle x_{s,q}(\{\phi_j(t)\})x_{s,q}^{\top}(\{\phi_j(t+\tau)\})\rangle$, then corresponds to the $q$th diagonal component of the matrix $C_s(\tau)$ in Equation (30); which we write $[C_s(\tau)]_{q,q}$ with corresponding power-density spectrum $\left[S^{(\nu)}\left(\omega_m^{(\nu)}\right)\right]_{q,q}$. The single-sided phase-noise spectrum of the C-OSC PSS state variable, $x_{s,q}$, is then defined as

$$\mathfrak{L}(\omega_m) = \left[S^{(1)}(\omega_m > 0)\right]_{q,q} / \|X_{s,1}^{[q]}\|^2 \tag{34}$$

where we have set $\omega_m^{(1)} = \omega_m$ for simplicity, $X_{s,\nu}$ denotes the $\nu$th harmonic of $x_s(t)$ and $X_{s,\nu}^{[q]} \in \mathbb{C}$ is the $q$th component of this complex vector *i.e.* $X_{s,\nu} = (X_{s,\nu}^{[1]}, X_{s,\nu}^{[2]}, ..., X_{s,\nu}^{[n]})^{\top} \in \mathbb{C}^n$. A closed-form expression for $\left[S^{(\nu)}(\omega_m^{(\nu)})\right]_{q,q}$ is derived in Equation (D12) of Appendix D. Inserting this expression, with $\nu = 1$, into Equation (34) gives the following closed-form expression for the single-sided phase-noise spectrum of a $k$-order C-OSC ensemble

$$\mathfrak{L}(\omega_m) = \frac{(1-a^{(1)})(\omega_0^2 c) - 2b^{(1)}\omega_m}{(0.5\omega_0^2 c)^2 + \omega_m^2} + \sum_{\rho}\sum_{l=2}^{k} \frac{\Upsilon_{l\rho}^{(1)}\left[2|\mu_{l,r}| + (\omega_0^2\rho^2 c)\right] + 2\Delta_{l\rho}^{(1)}\left[\omega_m + \mu_{l,i}\right]}{\left(|\mu_{l,r}| + (0.5\omega_0^2\rho^2 c)\right)^2 + \left(\omega_m + \mu_{l,i}\right)^2} \tag{35}$$

where the complex Floquet characteristic exponents have been written $\mu_l = \mu_{l,r} + j\mu_{l,i}$ and we have defined the parameters $a^{(\nu)} + jb^{(\nu)} = \left[\Omega^{(\nu)}\right]_{(q,q)} / \|X_{s,\nu}^{[q]}\|^2$, $\Upsilon_{l\rho}^{(\nu)} + j\Delta_{l\rho}^{(\nu)} = \left[\Theta_{l\rho}^{(\nu)}\right]_{(q,q)} / \|X_{s,\nu}^{[q]}\|^2$, with complex matrices $\Omega^{(\nu)}, \Theta_{l\rho}^{(\nu)} \in \mathbb{C}^{n\times n}$ calculated in Equations (D8)–(D9) of Appendix D (note: all sums w/o limits are assumed to go from $-\infty$ to $\infty$).

## 7 | NUMERICAL EXPERIMENTS

The C-OSC PMM model described above has been implemented numerically. Here, this software is used to investigate the phase-noise response of various coupled oscillator configurations detailed in Figures 3 and 7. The results thus obtained are then verified against simulations produced using the Keysight-ADS ©CAD circuit simulator. From Figure 3, we consider the two distinct injection-locked configurations INJ-OSC(1|2). These circuits are constructed by coupling the (XMF/VDP)-OSC units, at the respective injection ports ($v_{inj}$), through a simple unilateral polynomial transconductance amplifier. The simulations below, however, only consider linear coupling, that is, $g_{ci} = 0$ for $i \neq 1$, deferring the topic of nonlinear coupling to future work. The default circuit component values are printed in Figure 3. Given this default configuration, six parameter sets, three for each INJ-OSC configuration, are listed in Table 1. All simulations reported below correspond to one of the configurations listed in Table 1. An injection-locked configuration constitute a second-order ensemble (i.e., two coupled oscillator units, see Section 2). From the discussion in Section 3 above, this then implies the existence of a two-dimensional phase-manifold $\mathcal{P}$. Then, from Lemma 5.1, the phase LR is then governed by two distinct Floquet modes $(u_1(t) = \dot{x}_s(t), v_1(t), \lambda_1 = 1)$ and $(u_2(t), v_2(t), \lambda_2 < 1)$. The single-sided phase-noise spectrum then follows directly from the expression in Equation (35) with $k = 2$.

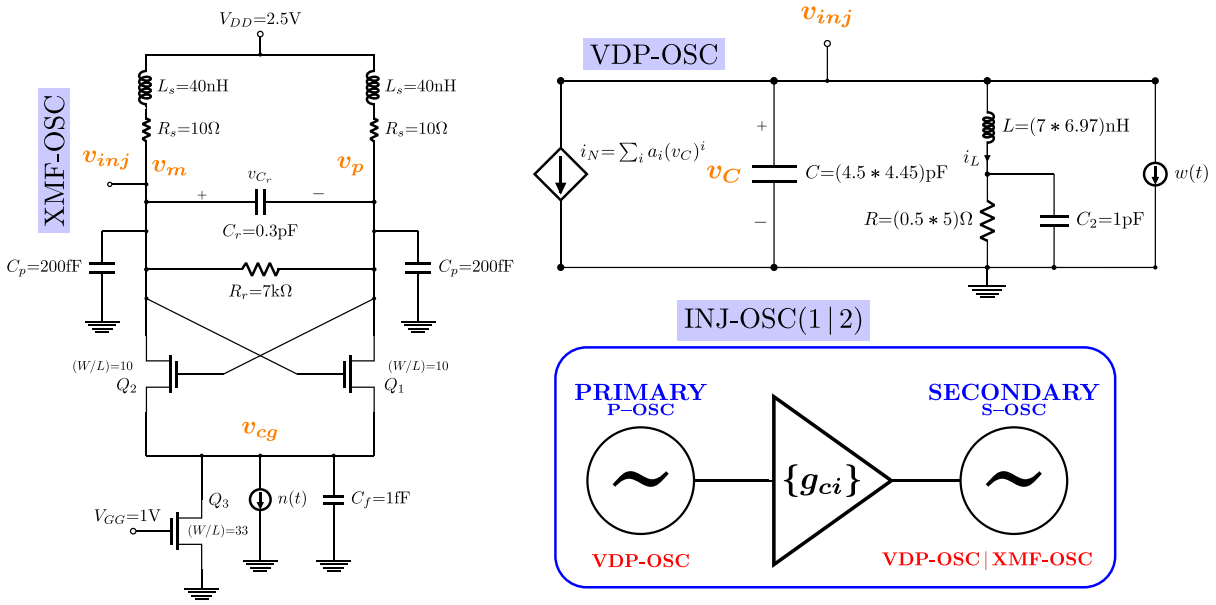


**FIGURE 3** The two oscillator units considered in experiments below, XMF-OSC: a MOSFET cross-coupled LC oscillator and VDP-OSC: a van-der-Pol type LC resonator unit. These are arranged in two injection-locked coupling arrangements INJ-OSC1 and INJ-OSC2. The VDP-OSC unit is considered both as *primary* (INJ-OSC1+2) and *secondary* (INJ-OSC1) oscillator with the component values listed as (primary-value ∗ secondary-value). Fixed default values: XMF-OSC current noise source (rms value) $n(t) = 70.7\text{pA}/\sqrt{Hz}$, VDP-OSC negative resistance polynomial coefficients $a_0 = a_2 = 0, a_1 = (1 * 5)\text{mA/V}$ and $a_3 = -(100 * 500)\mu\text{A/V}^3$, VDP-OSC noise source (rms value) $w(t) = 1.0(\text{pA} * \text{nA})/\sqrt{\text{Hz}}$. The coupling buffer is a polynomial trans-conductance amplifier $i_{\text{out}} = \sum g_{ci}(v_{\text{in}})^i$. In the default setting, all the coupling coefficients, except for the linear coupling $g_{c1}$, are set to zero $g_{ci} = 0.0$ for $i \neq 1$. The MOSFET transistors use the model reported in Maffezzoni et al.[34] The $v_{inj}$ ports in the above schematic serve as coupling input/output ports in all coupling configurations described below. All simulations include resistor and transistor noise sources [Colour figure can be viewed at wileyonlinelibrary.com]

**TABLE 1** The three parameter sets, P-SET #1–3 considered for the numerical experiments

| | INJ-OSC1 | INJ-OSC2 | BIC3-OSC |
|---|---|---|---|
| **P-SET #1** | $g_{c1}$=50$\mu$S | $g_{c1}$=40$\mu$S | $R_{c[1\|2\|3]} = [1.2\|1.4\|1.25]k\Omega$ |
| **P-SET #2** | $g_{c1}$=0.2$m$S | $g_{c1}$=70$\mu S$ | $R_{c[1\|2\|3]} = [2.9\|3.1\|2.95]k\Omega$ |
| **P-SET #3** | $g_{c1}$=1.0$m$S | $g_{c1}$=0.12$m$S | $R_{c[1\|2\|3]} = [3.4\|3.6\|3.45]k\Omega$ |

*Note*: All remaining parameters are fixed at the default values specified in Figures 3 and 7A.

The first step in the process of deriving the phase-noise spectra of the circuits in Figure 3 involves calculating corresponding the PSS solutions (i.e., the limit-cycles). This is done using a time-domain, Newton–Raphson iterative algorithm originally developed in Aprille and Trick.[35] The calculated PSS solutions for the INJ-OSC(1|2) circuits are shown in Figure 4 together with output of the frequency-domain Keysight-ADS ©PSS routine. Note that the two sets of solution curves have different phase-offsets which just represents that fact that the absolute phase (phase origin) of any oscillating systems is unspecified. Given this PSS solution, the corresponding Floquet decomposition $\{\lambda_i, u_i(t), v_i(t)\}$ is readily calculated using standard methods (see, e.g., other studies[5,6,31,36,37]) which in-turn allow us to calculate the various components of the expression in Equation (35) (see Appendix D). The resulting spectral curves are plotted in Figure 5. The figure plots spectra for both circuits in Figure 3 and all six parameter configurations are listed in Table 1. The results are compared against the output of the Keysight-ADS ©PNOISE-pnmx routine applied to the same circuits. The PNOISE-pnmx algorithm calculates the phase-noise spectrum using an FD-CM approach and hence represents an entirely independent method of verification.

Figure 6A shows the Floquet multiplier spectrum of the INJ-OSC2 circuit(P-SET #1) with the coupling, $g_{c1}$, being swept over the interval [38, 115]$\mu$A/V. Only relevant modes are shown in this figure. These are modes which satisfy $|\mathfrak{R}$

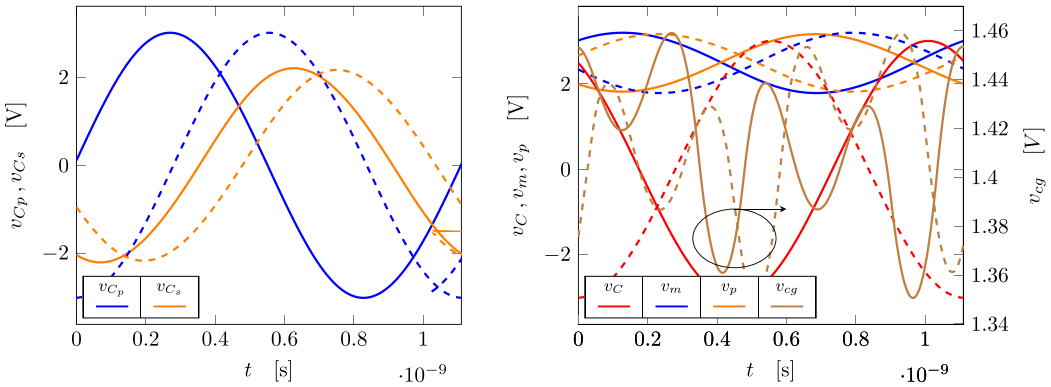


**(A)** INJ-OSC1 PSS **(B)** INJ-OSC2 PSS

**FIGURE 4** The PSS $x_s(t)$ for the two configurations INJ-OSC(1|2) detailed in Figure 3, for P-SET #1 listed in Table 1. The various nodes considered are indicated in Figure 3 in orange font. (A, B) $v_{C_{p/s}}$ = VDP-OSC $v_C$ node voltages of the (primary/secondary)(P/S)-OSC units in the INJ-OSC1 configuration. Solid line curves = in-house software, dashed line curves = Keysight-ADS ©PSS routine [Colour figure can be viewed at wileyonlinelibrary.com]

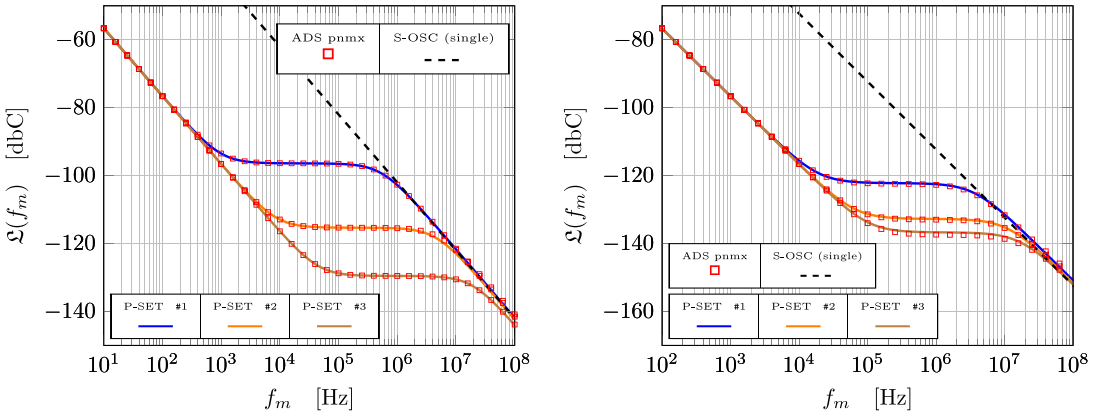


**(A)** INJ-OSC1 **(B)** INJ-OSC2

**FIGURE 5** The C-OSC single-sided phase-noise spectrum, derived in Equation (35), calculated for the two configurations INJ-OSC(1|2) detailed in Figure 3 and for the six parameter sets specified in Table 1. The calculated spectra (solid curves) are compared with the output of the Keysight-ADS © PNOISE (pnmx) routine (square symbols). The phase-noise spectra of the free-running S-OSC circuits are also included (dashed line) [Colour figure can be viewed at wileyonlinelibrary.com]

$\{\mu_i\}| \ll 2\pi f_0$ where $\mu_i$ are the Floquet exponents (see Section 2.3). The remaining seven modes ($\lambda_7 - \lambda_{14}$), not shown in this figure, are all of the magnitude $|\lambda_i|<10^{-8} \Rightarrow |\Re\{\mu_i\}|>18f_0$; referred to here as zero modes. It is a well-established fact that these zero-modes have no significant impact on the spectrum, for any reasonable frequency offset, and they can therefore safely be ignored.[34] The figure shows that two of the modes are stationary. These are modes associated with the P-OSC (driving) oscillator which of-course oscillates independently of the value taken by the unilateral coupling $g_{c1}$ (see Figure 3). The other four modes are connected to the S-OSC subcircuit response, and thus, all move around in the complex plane as the coupling changes; some more than others. From this figure, we identify two *phase-modes* $\lambda_1$, $\lambda_2$ and the four *amplitude modes* $\lambda_3, \lambda_4, \lambda_5 = \lambda_4^*, \lambda_6$. What follows is an explanation of this identification process. Firstly, $\lambda_1 = 1$ (red $\times$) is the stationary $\gamma$-phase-mode (see Section 2.3 and Equation 8). From Lemma 3.3, this mode is, by definition, a phase-mode. Secondly, the mode $\lambda_2$ is identified using Lemma 3.4 which prescribes that the limit $\lim_{g_{c1}\to 0}\lambda_2 = 1$ must be observed in order for it to be categorized as phase. Inspecting the figure, this limit is clearly observed. By the law of amplitude/phase dichotomy, that is, all that is not phase must be amplitude, the remaining four modes are categorized as amplitude.

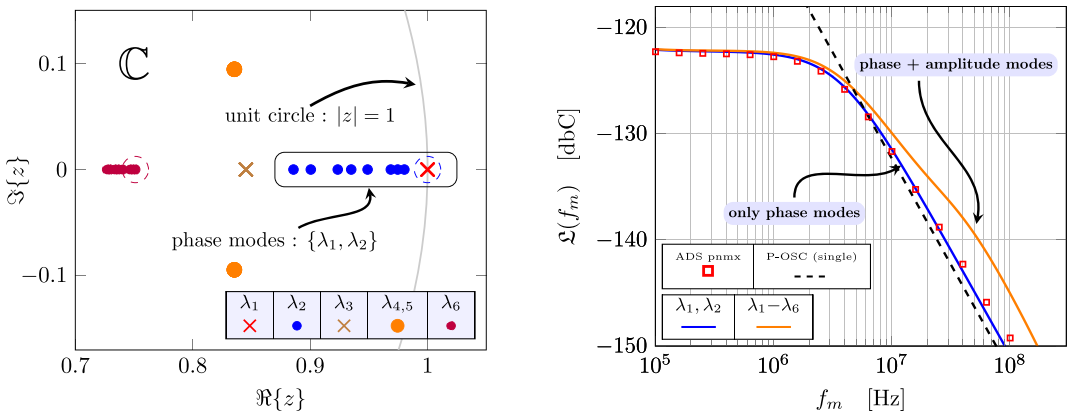


**(A)** INJ-OSC2 $\lambda$ spectrum **(B)** INJ-OSC2 (P-SET #1)

**FIGURE 6** (A) Floquet eigenvalue-spectrum of the the INJ-OSC2 circuit (P-SET #1) in the complex plane $\mathbb{C}$ as the coupling is varied in the interval $g_{c1} = 38 \rightarrow 115\mu$A/V. Symbols: $\times$ = stationary mode, dot = non-stationary (moving) mode, dashed circle = limit value of mode as $g_{c1} \rightarrow 0$. (B) The spectrum (same circuit/parameter set as in Figure 6A) is calculated using only the phase-modes, $\lambda_1$ and $\lambda_2$, (blue solid line) and by including the four amplitude modes $\lambda_1 - \lambda_6$ (orange solid line) [Colour figure can be viewed at wileyonlinelibrary.com]

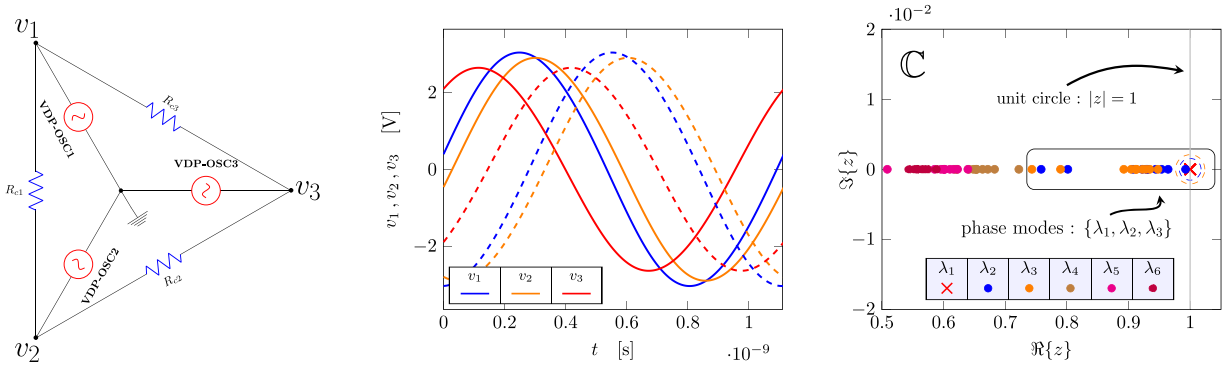


**(A)** BIC3-OSC **(B)** BIC3-OSC PSS **(C)** BIC3-OSC $\lambda$ spectrum

**FIGURE 7** (A) The BIC3-OSC circuit is constructed by bilaterally coupling 3 VDP-OSC units (see Figure 3) using the coupling resistors $R_{c[1-3]}$. VDP-OSC(1|2|3) component values: $C = (4.5|4.55|4.36)pF, R = (1.25|1.5|2)\Omega, L = (7|6.98|7.05)nH, w(t) = (2|3|5)\text{pA}/\sqrt{Hz}, a_0 = a_2 = 0$, $a_1 = 3\text{mA/V}$ and $a_3 = -300\mu\text{A/V}^3$. (B) The calculated PSS solution compared with the equivalent ADS-Keysight result. Plot legends: see Figure 4 caption. (C) The BIC3-OSC Floquet mode spectrum for varying values of the coupling strength (controlled by the three coupling resistors $R_{c[1|2|3]}$). Plot legends: see Figure 6A caption [Colour figure can be viewed at wileyonlinelibrary.com]

Figure 6B then investigates the result of including these four amplitude modes into the calculation phase-noise spectrum. For lower offsets, the plots follow each other as the output is dominated by the phase-mode response. However, at higher offsets, the amplitude contributions gain importance and the two spectra begin to diverge. This experiment serve as a direct demonstration that there indeed does exist dedicated phase-modes for coupled systems as predicted by the novel C-OSC PMM proposed herein. For second-order ensemble circuits INJ-OSC(1|2), the model predicts that two dedicated phase-modes must exist following from the two-dimensional phase-manifold $\mathcal{P}$ governing the asymptotic dynamics of these circuits. Figure 6B directly verifies this prediction. When the spectrum is calculated using the phase-modes $\lambda_1$ and $\lambda_2$, it follows the PNOISE-pnmx reference for all offsets of interest. However, when the amplitude modes are added, the spectrum diverges from this reference introducing gap at some offset reaching around $3-4$ dB which obviously represents a significant and observable discrepancy.

Figure 7A shows the BIC3-OSC circuit built from 3 VDP-OSC units (see Figure 3) coupled bilaterally, in a global coupling configuration, using resistive coupling components. The circuit represents a third-order ensemble (i.e., $k = 3$)

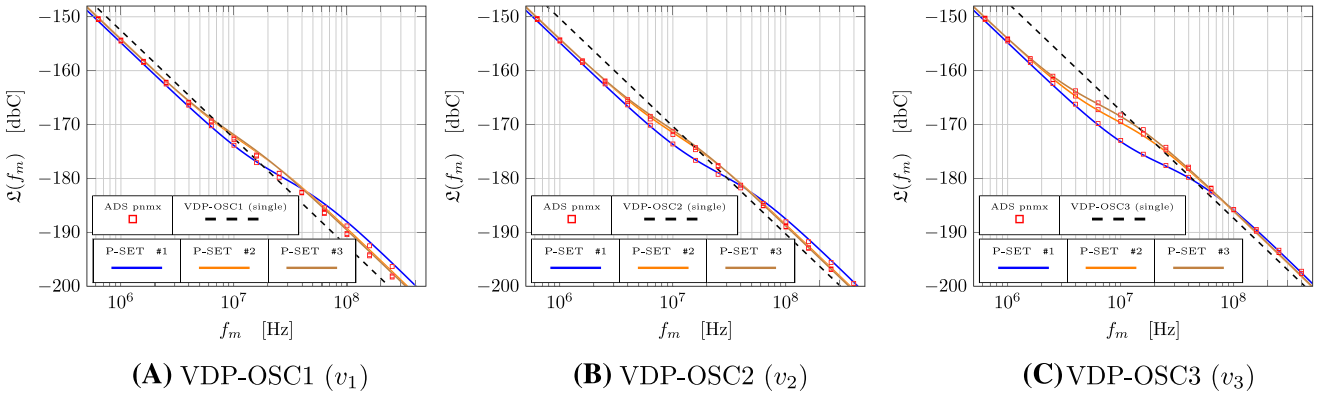


**FIGURE 8** The C-OSC single-sided phase-noise spectrum for the three output nodes of the BIC3-COUP circuit in Figure 7A for the three parameter sets in Table 1 (see also Figure 5 caption) [Colour figure can be viewed at wileyonlinelibrary.com]

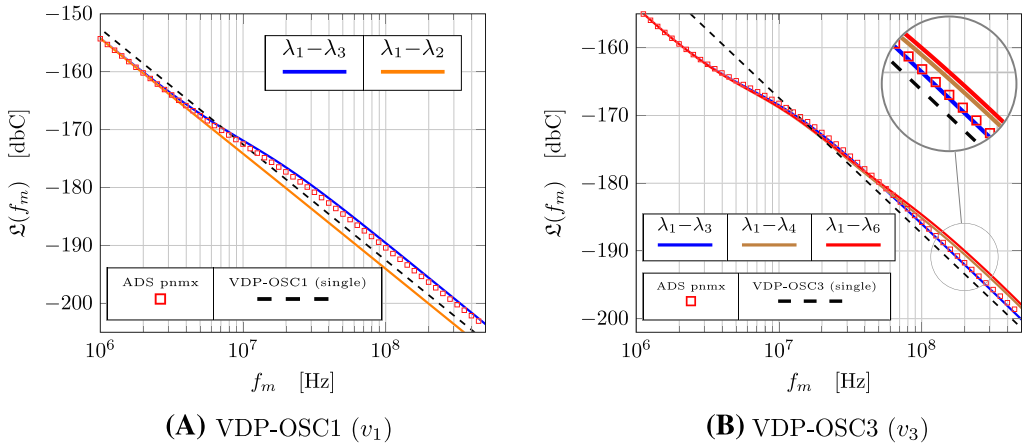


**FIGURE 9** The C-OSC single-sided phase-noise spectrum for the BIC3-COUP circuit in Figure 7A calculated using various combinations of the nonzero Floquet modes $\lambda_1 - \lambda_6$ shown in Figure 7C. The curves are calculated for parameter set PSET-3 defined in Table 1 for output nodes: (A) $= v_1$ and (B) $= v_3$ (see also Figure 6B caption) [Colour figure can be viewed at wileyonlinelibrary.com]

and the model developed above in Sections 3–6 then predicts that three dedicated phase-modes must exist governing the weak-noise dynamics on the three-dimensional phase-manifold $\mathcal{P}$. Below, a series of numerical experiments involving this circuit are conducted for the three sets of circuit parameters PSET#1–3 listed in Table 1; the remaining parameters held fixed at the values specified in Figure 7A caption. These experiments directly mirror the simulations discussed above for the INJ-OSC(1|2) circuits. The discussion below will therefore often refer back to Figures 4–6 and the corresponding text in order to avoid repeating the same points twice.

Figure 7B compares the calculated BIC3-OSC PSS curves with corresponding Keysight-ADS results, for the parameter set PSET #3 as specified in Table 1, and for each of the three BIC3-OSC output-nodes $v_{1\_3}$. Figure 7C shows the BIC3-OSC Floquet spectrum as a function of varying the coupling strength of the network. This spectrum contains six nonzero modes $\lambda_1 - \lambda_6$; ignoring the remaining three zero-modes (see discussion above). As the BIC3-OSC circuit constitutes a third-order ensemble, the model predicts the existence of three dedicated phase-modes. Figure 7C identifies these as the set $\lambda_1 - \lambda_3$ with the remaining modes $\lambda_4 - \lambda_6$ then describing BIC3-OSC amplitude. Figure 8 plots the phase-noise spectra at each of the three output nodes $v_{1\_3}$ for each of the three parameter sets PSET#1–3. The figure shows curves calculated using C-OSC single-sided phase-noise model in Equation (35) ($k = 3$) together with the equivalent spectra produced running the frequency-domain ADS-Keysight ©PNOISE-pnmx algorithm.

Finally, Figure 9 investigates the effects of applying other mode combinations to compute the phase-noise spectra. Figure 9A shows the result of including only two of the three dedicated phase-modes. It clearly illustrates how this choice introduces a significant error (around 4 dB) in the calculated spectrum of the $v_1$ node. Figure 9B then shows the

result of adding the amplitude modes $\lambda_4 - \lambda_6$ in the calculation of the $v_3$ node spectrum. The curves show a distinct introduced error at higher offsets in the range $1.5 - 2$ dB. The figure illustrate a clear trend that including more amplitude modes leads to a more significant error contribution. For the BIC3-OSC circuit (third-order ensemble), the COSC-PMM model predicts that three dedicated phase-modes must exist, following from the three-dimensional phase-manifold $\mathcal{P}$. The three modes then govern the asymptotic phase-noise response of this circuit. The experiments detailed in Figure 9 directly verify this prediction. When the spectrum is calculated using all three phase-modes, $\{\lambda_1, \lambda_2, \lambda_3\}$, it follows the PNOISE-pnmx simulation for all offsets of interest. However, when some of the phase-modes are neglected (Figure 9A) or when amplitude modes are added (Figure 9B), the spectrum tends to diverge from this reference at higher offset frequencies.

## 8 | CONCLUSION

We present a novel macro-model aimed at predicting phase-noise performance of a general coupled synchronized oscillator ensemble perturbed by weak noise sources. The proposed framework is generalized and can be applied to all circuit and coupling configurations. To the authors knowledge, the work herein represents the first attempt at this sort of macro-modeling strategy applied general coupled oscillator scenarios.

The proposed model predicts that a $k$-order ensemble of coupled oscillators will imply $k$ dedicated modes governing the stochastic phase-response of the ensemble, that is, the *k-phase-modes*. The remaining modes are then categorized as amplitude modes. The prediction put forth by the proposed model was subsequently verified in a series of numerical experiments which compared our results with the output of the Keysight-ADS ©PNOISE-pnmx routine.

In radar/remote-sensing and RF/$\mu$-wave communication systems, the BER of the received signal is directly linked to the phase-noise performance of the system clocks/oscillators. The demand for rigorous, and computationally efficient, modeling solutions is hence obvious. The macro-model proposed herein shows great potential for industry application as it is completely generalized and allows for easy integration into existing computer-aided design (CAD) simulation environments.

### ACKNOWLEDGMENT

The authors gratefully acknowledge partial financial support by German Research Foundation (DFG) (Grant KR 1016/16-1).

### DATA AVAILABILITY STATEMENT

Research data are not shared.

### ORCID

*Torsten Djurhuus* https://orcid.org/0000-0003-1916-7647
*Viktor Krozer* https://orcid.org/0000-0002-2387-1947

### REFERENCES

1. Ilias C, Domenico P, Domenico Z. Analyses and techniques for phase noise reduction in CMOS Colpitts oscillator topology. *Int J Circuit Theory Appl*. 2016;44(3):616-638.
2. Bica OL, Ahmed A, Filanovsky Igor M, Fernandes JR, Verhoeven CJM, Silva MM. Experimental comparison of phase-noise in cross-coupled RC-and LC-oscillators. *Int J Circuit Theory Appl*. 2010;38(7):681-688.
3. Geraedts PFJ, Ed T, Klumperink Eric AM, Wienk GJM, Bram N. Towards minimum achievable phase noise of relaxation oscillators. *Int J Circuit Theory Appl*. 2014;42(3):238-257.
4. Pankratz E, Sánchez-Sinencio E. Survey of integrated-circuit-oscillator phase-noise analysis. *Int J Circuit Theory Appl*. 2014;42(9):871-938.
5. Kärtner FX. Analysis of white andf−α noise in oscillators. *Int J Circuit Theory Appl*. 1990;18(5):485-519.
6. Alper D, Amit M, Jaijeet R. Phase noise in oscillators: A unifying theory and numerical methods for characterization. *IEEE Trans Circuits Syst I: Fund Theory Appl*. 2000;47(5):655-674.
7. Traversa FL, Fabrizio B. Oscillator noise: A nonlinear perturbative theory including orbital fluctuations and phase-orbital correlation. *IEEE Trans Circuits Syst I: Reg Pap*. 2011;58(10):2485-2497.
8. Torsten D, Viktor K, Jens V, Johansen Tom K. Oscillator phase noise: A geometrical approach. *IEEE Trans Circuits Syst I: Reg Pap*. 2009;56(7):1373-1382.

9. Shwetabh V, Rategh Hamid R, Lee Thomas H. A unified model for injection-locked frequency dividers. *IEEE J Solid-State Circuits*. 2003; 38(6):1015-1027.
10. Xiangdong Z, Xuesong Z, Daryoush Afshin S. A theoretical and experimental study of the noise behavior of subharmonically injection locked local oscillators. *IEEE Trans Microw Theory Techniq*. 1992;40(5):895-902.
11. Behzad R. A study of phase noise in CMOS oscillators. *IEEE J Solid-State Circuits*. 1996;31(3):331-343.
12. Xudong C, York RA. Coupled-oscillator scanning technique for receiver applications. In: 1311–1314 IEEE; 1995.
13. Shen J, Wilson PL. A design for a two-dimensional coupled oscillator beam-steering antenna array. *IEEE Antennas Wirel Prop Lett*. 2003;2:360-362.
14. Pogorzelski RJ. On the dynamics of two-dimensional array beam scanning via perimeter detuning of coupled oscillator arrays. *IEEE Trans Antennas Propag*. 2001;49(2):234-242.
15. Hsiang-Hui C, I-Hui H, Shen-Iuan L. A spread-spectrum clock generator with triangular modulation. *IEEE J Solid-State Circuits*. 2003; 38(4):673-676.
16. Kenji K, Tsuneo T, Masayoshi A. Injection-locked oscillator chain: A possible solution to millimeter-wave MMIC synthesizers. *IEEE Trans Microw Theory Tech*. 1997;45(9):1578-1584.
17. York RA, Compton RC. Quasi-optical power combining using mutually synchronized oscillator arrays. *IEEE Trans Microw Theory Tech*. 1991;39(6):1000-1009.
18. York RA, Compton RC. Coupled-oscillator arrays for millimeter-wave power-combining and mode-locking. In: 429–432 IEEE; 1992.
19. Kaertner FX. Determination of the correlation spectrum of oscillators with low noise. *IEEE Trans Microw Theory Tech*. 1989;37(1): 90-101.
20. Heng-Chia C, Xudong C, Mishra Umesh K, York RA. Phase noise in coupled oscillators: Theory and experiment. *IEEE Trans Microw Theory Tech*. 1997;45(5):604-615.
21. Heng-Chia C, Xudong C, Vaughan Mark J, Mishra Umesh K, York Robert A. Phase noise in externally injection-locked oscillator arrays. *IEEE Trans Microw Theory Tech*. 1997;45(11):2035-2042.
22. Djurhuus T, Krozer V, Vidkjar J, Johansen TK. Trade-off between phase-noise and signal quadrature in unilaterally coupled oscillators. In: 883–886 IEEE; 2005.
23. Djurhuus T, Krozer V, Vidkjær J, Johansen TK. Nonlinear analysis of a cross-coupled quadrature harmonic oscillator. *IEEE Trans Circuits Syst I: Reg Pap*. 2005;52(11):2276-2285.
24. Djurhuus T, Krozer V, Vidkjær J, Johansen TK. AM to PM noise conversion in a cross-coupled quadrature harmonic oscillator. *Int J RF Microw Computer-Aided Eng*. 2006;16(1):34-41.
25. Ramirez F, Ponton M, Sancho S, Suarez A. Phase-noise analysis of injection-locked oscillators and analog frequency dividers. *IEEE Trans Microw Theory Tech*. 2008;56(2):393-407.
26. Djurhuus T, Krozer V. Theory of injection-locked oscillator phase noise. *IEEE Trans Circuits Syst I: Reg Pap*. 2010;58(2):312-325.
27. Hirsch Morris W, Pugh CC. Shub Michael. Invariant manifolds. *Bull Am Math Soc*. 1970;76(5):1015-1019.
28. Hirsch Morris W, Pugh CC, Shub M. *Invariant manifolds*. Springer; 2006.
29. Mañé R, others. Persistent manifolds are normally hyperbolic. *Bull Am Math Soc*. 1974;80(1):90-91.
30. Mané R. Persistent manifolds are normally hyperbolic. *Trans Am Math Soc*. 1978;246:261-283.
31. Alper D. Floquet theory and non-linear perturbation analysis for oscillators with differential-algebraic equations. *Int J Circuit Theory Appl*. 2000;28(2):163-185.
32. Frankel T. *The geometry of physics: an introduction*. Cambridge university press; 2011.
33. Lee JM. *Smooth manifolds*. Springer; 2013:1-31.
34. Maffezzoni P, Pepe F, Bonfanti A. A unified method for the analysis of phase and amplitude noise in electrical oscillators. *IEEE Trans Microw Theory Tech*. 2013;61(9):3277-3284.
35. Aprille TJJR, Trick T. A computer algorithm to determine the steady-state response of nonlinear oscillators. *IEEE Trans Circuit Theory*. 1972;19(4):354-360.
36. Alper D, Jaijeet R. A reliable and efficient procedure for oscillator PPV computation, with phase noise macromodeling applications. *IEEE Trans Computer-Aided Des Integr Circuit Syst*. 2003;22(2):188-197.
37. Traversa FL, Fabrizio B. Improved harmonic balance implementation of Floquet analysis for nonlinear circuit simulation. *AEU-Int J Electron Commun*. 2012;66(5):357-363.
38. Fenichel N, Moser JK. Persistence and smoothness of invariant manifolds for flows. *Ind Univ Math J*. 1971;21(3):193-226.


**How to cite this article:** Djurhuus T, Krozer V. A generalized model of coupled oscillator phase-noise response. *Int J Circ Theor Appl*. 2021;1-21. doi:10.1002/cta.3139

## APPENDIX A: INVARIANCE OF FLOQUET SUB-BUNDLES

We consider the $q$-dimensional Floquet sub-bundle

$$\mathcal{U} = \text{span}\{u_{i_1}(\eta), u_{i_2}(\eta), ...u_{i_q}(\eta)\} \tag{A1}$$

spanned by $q$ Floquet vectors $\{u_i(\eta)\}$, $\eta \in [0, T_0]$.

**Lemma A.1.** The Floquet sub-bundle $\mathcal{U}$ is mapped invariantly by the flow, that is, $d\psi_t(\mathcal{U}) \subset \mathcal{U}$.

*Proof.* Let $\sigma \in \mathcal{U}$ represent an initial condition in this sub-bundle at $\eta = s$ written as $\sigma = \sum_{p=1}^{k} a_p u_{i_p}(s)$. This vector is then mapped (pushed-forward) by the LR flow $\sigma^* = d\psi_t(\sigma)$. From Section 2.3, the mapped response has the form $\sigma^* = \sum_{p=1}^{q} b_{i_p} u_{i_p}(t) \in \mathcal{U}$ with $b_r = a_r \exp(\mu_r(t-s))$.

**Lemma A.2.** Any $q$-dimensional sub-bundle $\mathcal{Z}$, mapped invariantly by the flow $d\psi_t(\mathcal{Z}) \subset \mathcal{Z}$, correspond to a unique $q$-dimensional Floquet representation $\mathcal{U}$.

*Proof.* Let $\mathcal{Z} = \text{span}\{z_1(\eta), z_2(\eta), ...z_q(\eta)\}$ with $\{z_i(\eta)\}$ some set of unspecified vector-functions. The $n$-dimensional Floquet set $\{u_i(\eta)\}$ is complete, and we can expand $z_j(\eta) = \sum_{m=1}^{N_j} \alpha_j^m(\eta) u_{i_m}(\eta)$ where $\alpha_j^m(\eta)$ are the expansion functions and $1 \le N_j \le n$ is the dimension of the expansion. As the modes $\{u_i(\eta)\}$ are linear-independent, we get $\mathcal{Z} = \text{span}\{u_{i_1}(\eta), u_{i_2}(\eta), ...u_{i_Q}(\eta)\}$ where $q \le Q \le n$ is the dimension of the bundle. However, as $\mathcal{Z}$ was assumed to be a $q$-dimensional bundle, we must have $Q = q$ which implies $\mathcal{Z} = \mathcal{U}$ as defined in Equation (A1).

## APPENDIX B: VARIOUS LEMMA PROOFS

Proof of Lemma 3.1: we can write $\mathcal{P}_0 = \gamma_1 \times \gamma_2 \times ... \times \gamma_k$ where $\gamma_i$ is the limit-cycle manifold corresponding to the $i$th uncoupled oscillator unit in the ensemble. This manifold is $k$-dimensional; being the product of $k$ 1-D manifolds. It is a compact, NH, smoothly embedded (i.e., has a smooth coordinate description) manifold as each component in product (the limit-cycles $\gamma_i$) is compact, NH and smoothly embedded. Let the uncoupled flow be written $\psi_t = \psi_t^{(1)} \bigotimes \psi_t^{(2)} \bigotimes ... \bigotimes \psi_t^{(k)}$, where $\psi_t^{(i)}$ is the flow of the $i$th uncoupled, free-running, oscillator. The limit-cycle $\gamma_i$, being a $\omega$-limit set, is, by definition, an invariant of the flow $\psi_t^{(i)}$ and from Equation (15), $\psi_t(\mathcal{P}_0) = \psi_t^{(1)} \bigotimes \psi_t^{(2)} \bigotimes ... \bigotimes \psi_t^{(k)}(\gamma_1, \gamma_2, ..., \gamma_k) = \psi_t^{(1)}(\gamma_1) \times \psi_t^{(2)}(\gamma_2) \times ... \times \psi_t^{(k)}(\gamma_k) \subset \mathcal{P}_0$. By definition, the periodic one-dimensional limit-sets $\gamma_i$ are diffeomorphic to the simple circle $\gamma_i \cong \mathbb{S}, i = 1, 2, ...k$. Inserting this into Equation (15), it follows that $\mathcal{P}_0 \cong \mathbb{T}^k = \mathbb{S} \times \mathbb{S} \times ... \times \mathbb{S}$ ($k$ times).

Proof of Lemma 3.2: From Lemma 3.1, the zero coupling, $\epsilon = 0$, manifold $\mathcal{P}_0$ is a compact NHIM. It is an established fact[27–30] (see summary in Appendix C) that this manifold is persistent. The manifold is hence known to survive under a weak deformation mapping, in terms of the parameter $\epsilon$. As the phase-manifold $\mathcal{P}$ is a smooth deformation of embedded manifold $\mathcal{P}_0$, it follows trivially that $\mathcal{P}$ is also smoothly embedded in $\mathcal{X}$ (i.e., has a smooth coordinate representation). From Lemma 3.1, we have $\mathcal{P}_0 \cong \mathbb{T}^k$. Then, since $\mathcal{P}$ is a smooth deformation (i.e., $\mathcal{P} \cong \mathcal{P}_0$), it follows directly that $\mathcal{P} \cong \mathcal{P}_0 \cong \mathbb{T}^k \Rightarrow \mathcal{P} \cong \mathbb{T}^k$.

Proof of Lemma 3.4: The deformation of the uncoupled phase-manifold $\mathcal{P}_0$ into $\mathcal{P}$ preserves fiber structure[27–30] (see summary in Appendix C). Hence, the Floquet modes spanning the bundle $\mathsf{T}_\gamma \mathcal{P}$ are continuously and smoothly deformed from the tangent-bundle $\mathsf{T}\mathcal{P}_0$. However, the dynamics on the uncoupled bundle $\mathsf{T}\mathcal{P}_0$ is neutrally stable in all $k$ directions; as the individual limit-circles in the product (15) are neutrally stable for directions tangent to this set. Then, as the Floquet modes are deformed smoothly and continuously from this setting, the limit rule follows.

Proof of Lemma 4.1: From Lemma 3.2, the phase-manifold $\mathcal{P}$ is a $k$-dimensional compact manifold embedded in $\mathcal{X}$. Here ,$\mathcal{S} \subset \mathcal{X}$ is an open subset containing $\mathcal{P}$. It then follows that $\mathcal{P}$ is also embedded in $\mathcal{S}$; that is, a regular submanifold. There then exist a smooth coordinate system $w = (a, b) \in \mathbb{R}^n$ where $\mathcal{P}$ is represented by the $k$-slice $b = \mathbf{0} = (0, 0, ..., 0)$ ($n - k$ times)[32,33]; that is, $\mathcal{P}$ is parameterized by the $k$ coordinates $a \in \mathbb{R}^k$. From Lemma 3.2, it further follows that $\mathcal{P}$ is

diffeomorphic (smoothly related) to the $k$-torus $\mathcal{P} \cong \mathbb{T}^k$ which implies that all $a$-coordinates must be periodic. Equivalently, the coordinates $b \in \mathbb{R}^{n-k}$ cannot be periodic since they map to points off $\mathcal{P}$. The 1-D limit-cycle $\gamma$ is smoothly embedded in $\mathcal{P}$ and is hence parameterized by a single-phase coordinate. Here, we choose first coordinate ($\phi_1$) in the vector $a \in \mathbb{R}^k$ to parameterize this set.

## APPENDIX C: PERSISTENCE OF NH INVARIANT MANIFOLDS: A SUMMARY OF ESTABLISHED THEORY

The concept of an NHIM can be traced to a 1971 paper[38] by Fenichel and Moser. Below, we give a short review of this subject. For readers interested in more thorough discussion of this subject, we refer to the literature.[27–30,38] Let $g : \mathcal{M} \to \mathcal{M}$ be the time-one map of the flow restricted to $\mathcal{M}, g(x) = \psi_{t=1}(x), x \in \mathcal{M}$ and let $g^i$ be the $i$th iteration of this diffeomorphism $g^i(x) = g \circ g ... \circ g(x)$ (i times). Then, $dg_x$ denotes the differential (Jacobian) of $g$ at $x \in \mathcal{M}$ and the Jacobian of the $i$th iterate becomes $dg^i(x) = d(g \circ g ... \circ g(x)) = dg_x \circ dg_x ... \circ dg_x = (dg_x)^i$. Letting $v_t \in \mathsf{T}_y\mathcal{M}$ be a vector tangent to $\mathcal{M}$ at $y = g^i(x) \in \mathcal{M}$ and $v_p \notin \mathsf{T}_x\mathcal{M}$ be a vector traverse to $\mathcal{M}$ based at $x \in \mathcal{M}$ then $\mathcal{M}$ is a NHIM if there exists positive real constants $K > 0$ and $0 < \lambda < 1$ such that for $i \in \mathbb{Z}_+$ we have[27-30]

$$\begin{aligned} \|(dg_x)^i v_p\| &\le K\lambda^i \\ \|(dg_x)^i v_p\| \cdot \|(dg_y)^{-i} v_t\| &\le K\lambda^i \end{aligned} \tag{C2}$$

The expressions in Equation (C2) state, loosely speaking, that the contraction in directions normal to this space exceeds the corresponding tangential contraction. Hence, orbits starting on $\mathcal{M}$ contract slower than orbits with initial conditions off $\mathcal{M}$. For this reason, a NHIM manifold is sometimes referred to as a *slow-manifold*. The concept of $\mathcal{C}^1$-closeness is now introduced.

**Definition C.1.** Two maps $f$, $g$, with domain $\mathcal{B}$, are said to be $\mathcal{C}^1$ $\kappa$-*close* if both the maps themselves as well as their derivatives are $\kappa$-close, that is, $\sup_{x \in \mathcal{B}} \|f(x) - g(x)\| \le \kappa$ and $\sup_{x \in \mathcal{B}} \|Df_x - Dg_x\| \le \kappa$ for some small $|\kappa| \ll 1$.

which leads to

**Definition C.2.** Two $q$-dimensional embedded manifolds $\mathcal{M}, \mathcal{N} \subset \mathcal{X}$ are said to be $\mathcal{C}^1$ $\kappa$-close if the corresponding coordinate maps $x : \mathcal{M} \to \mathbb{R}^q$ and $y : \mathcal{N} \to \mathbb{R}^q$ are $\mathcal{C}^1$ $\kappa$-close.

Given these definitions, the concept of a *persistent invariant manifold*, on state-space $\mathcal{X} \subset \mathbb{R}^n$, can be stated.[29,30]

**Definition C.3.** Let $f, g : \mathbb{R}^n \to \mathbb{R}^n$ be two smooth $\mathcal{C}^1$ $\kappa$-close vector fields on $\mathcal{X}$ with corresponding flows $\psi_t, \tilde{\psi}_t : \mathbb{R}^n \times \mathbb{R} \to \mathbb{R}^n$ and assume that the embedded manifold $\mathcal{M} \in \mathcal{X}$ is invariant under the flow $\psi_t$. Then, $\mathcal{M}$ is said to be *persistent* if there exist a smooth $\kappa$-close embedded manifold $\mathcal{N}$ invariant under $\tilde{\psi}_t$.

Persistence preserves smoothness and fiber structure.[29,30] For a *compact* NHIM, we have

**Theorem C.1.** *Let $\mathcal{M}$ be a compact manifold w/o boundary, then it follows*

$$\mathcal{M} \text{ is a NHIM} \Leftrightarrow \mathcal{M} \text{ is persistent} \tag{C3}$$

*Proof.* The $\Rightarrow$ part of this theorem was proven in Hirsch Morris and Pugh,[27,28] whereas reverse statement $\Leftarrow$ was proven in Mañé.[29,30]

## APPENDIX D: THE C-OSC PHASE SPECTRUM

The vector $\lambda_i : \mathbb{R} \to \mathbb{C}^n$ is now defined

$$\lambda_i(\eta) = \nu_i^{\top}(\eta) b(x_s(\eta)),\ i = 1,2,\ldots,k \tag{D4}$$

which is $T_0$-periodic and represents noise component corresponding to the $i$th Floquet mode $u_i$. Expanding the brackets of the phase correlation matrix, $C_s(\tau)$, defined in Equation (31) of Section 6, gives

$$C_s(\tau) = Q_s(\tau) + \sum_{m=1}^{k}[K_m(\tau) + J_m(\tau)] + \sum_{i=1}^{k}\sum_{m=1}^{k} P_{im}(\tau) \tag{D5}$$

with $Q_s(\tau) = \langle x_s(t+\alpha(t)) x_s^{\dagger}(t+\tau+\alpha(t+\tau)) \rangle, K_m(\tau) = \langle x_s(t+\alpha(t)) w_m^{\dagger}(t+\tau+\alpha(t+\tau)) \rangle$, $J_m(\tau) = \langle w_m(t+\alpha(t)) x_s^{\dagger}(t+\tau+\alpha(t+\tau)) \rangle$ and $P_{im}(\tau) = \langle w_i(t+\alpha(t)) w_m^{\dagger}(t+\tau+\alpha(t+\tau)) \rangle$. From Equation (32) and Equations (27)–(29), these matrices involve ensemble averages of Floquet modes and various complex stochastic integrals. Rigorous techniques for solving these types of stochastic integral expressions were developed in other studies.[5–7] From the calculations detailed in Traversa and Fabrizio,[7] we derive the following closed-form expressions for the correlation matrices in Equation (D5) for $\tau \geq 0$

$$\begin{aligned}
Q_s(\tau) &= \sum_r X_{s,r} X_{s,r}^{\dagger} \exp(-jr\omega_0\tau)\exp(-0.5\omega_0^2 r^2 c\tau) \\
P_{im}(\tau) &= \sum_{\rho}\sum_{p}\sum_{r} \frac{U_{i,p}\Lambda_{i,\rho-p}^{\top}\Lambda_{m,\rho-r}^{*}U_{m,r}^{\dagger}}{j\omega_0(r-p)-\mu_i-\mu_m^{*}} \exp(-0.5\omega_0^2\rho^2 c\tau)\exp(-jr\omega_0\tau)\exp(\mu_m^{*}\tau) \\
K_m(\tau) &= \sum_{\rho}\sum_{r} \frac{j\rho\omega_0 X_{s,\rho}\Lambda_{1,0}^{\top}\Lambda_{m,\rho-r}^{*}U_{m,r}^{\dagger}}{-j\omega_0(\rho-r)-\mu_m^{*}} [\exp(-jr\omega_0\tau)\exp(\mu_m^{*}\tau) - \exp(-j\rho\omega_0\tau)]\exp(-0.5\omega_0^2\rho^2 c\tau)
\end{aligned} \tag{D6}$$

whereas $J_m(\tau) = 0$ for $\tau \geq 0$.[7] In the above expressions $\Lambda_{i,r}$, $U_{i,r}$, and $X_{s,r}$ denote the $r$th harmonic of the vector $\lambda_i$ in Equation (D4), the Floquet mode $u_i(t)$ and the steady-state vector $x_s(t)$, respectively. In Equation (D6), and throughout, all sums w/o limits are assumed to go from $-\infty$ to $\infty$. From Equation (D5), the $\nu$th envelope in the expansion (33) is written $C_s^{(\nu)}(\tau) = Q_s^{(\nu)}(\tau) + K_m^{(\nu)}(\tau) + J_m^{(\nu)}(\tau) + P_{im}^{(\nu)}(\tau)$ and from Equation (D6)

$$C_s^{(\nu)}(\tau) \underset{\tau \geq 0}{=} \left[X_{s,\nu}^{*} X_{s,\nu}^{\top} - \Omega^{(\nu)}\right] \exp\left(-0.5\nu^2\omega_0^2 c|\tau|\right) + \sum_{\rho}\sum_{m=2}^{k} \Theta_{m\rho}^{(\nu)} \exp\left(-0.5\rho^2\omega_0^2 c\tau\right)\exp(\mu_m^{*}\tau) \tag{D7}$$

with the complex matrices $\Omega^{(\nu)}, \Theta_{m\rho}^{(\nu)} \in \mathbb{C}^{n\times n}$ defined as

$$\Omega^{(\nu)} = \sum_{m=2}^{k}\sum_{r} \frac{U_{1,\nu}\Lambda_{1,0}^{\top}\Lambda_{m,\nu-r}^{*}U_{m,r}^{\dagger}}{j\omega_0(r-\nu)-\mu_m^{*}} \tag{D8}$$

and

$$\Theta_{m\rho}^{(\nu)} = \frac{U_{1,\rho}\Lambda_{1,0}^{\top}\Lambda_{m,\rho-\nu}^{*}U_{m,\nu}^{\dagger}}{j\omega_0(\nu-\rho)-\mu_m^{*}-\mu_1} + \frac{\sum_{i=2}^{k}\sum^{p} U_{i,p}\Lambda_{i,\rho-p}^{\top}\Lambda_{m,\rho-\nu}^{*}U_{m,\nu}^{\dagger}}{j\omega_0(\nu-p)-\mu_m^{*}-\mu_i} \tag{D9}$$

where we have used the identities $U_{1,\rho} = j\rho\omega_0 X_{s,\rho}$ and $\mu_1 = 0$ (see Equation 8 in Section 2.3). From Equation (30), $C_s^{\top}(\tau) = \lim_{t\to\infty}\langle x_{\mathrm{LR}}(\{\phi_j(t)\}) x_{\mathrm{LR}}^{\top}(\{\phi_j(t+\tau)\})\rangle = \lim_{t\to\infty}\langle x_{\mathrm{LR}}(\{\phi_j(t_1)\}) x_{\mathrm{LR}}^{\top}(\{\phi_j(t_1-\tau)\})\rangle = C_s(-\tau)$ where $t_1 = t+\tau$ and we have used the stationary property of the asymptotic dynamics. Using this result and the envelope expansion in Equation (33), one finds $C_s^{\top}(\tau) = \sum_{\nu}\left(C_s^{(\nu)}(\tau)\right)^{\top}\exp(-j\nu\omega_0\tau) = C_s(-\tau) = \sum_{\nu} C_s^{(\nu)}(-\tau)\exp(j\nu\omega_0\tau) \Rightarrow C_s^{(\nu)}(-\tau) = \left(C_s^{(\nu)}(\tau)\right)^{\dagger}$ and the $\nu$th harmonic cross-power density spectrum is then written

$$S^{(\nu)}\left(\omega_m^{(\nu)}\right)=\int_{-\infty}^{\infty}C_s^{(\nu)}(\tau)\exp\left(-j\omega_m^{(\nu)}\tau\right)d\tau=\int_{0}^{\infty}\left[C_s^{(\nu)}(\tau)\exp\left(-j\omega_m^{(\nu)}\tau\right)+\left(C_s^{(\nu)}(\tau)\right)^{\dagger}\exp\left(j\omega_m^{(\nu)}\tau\right)\right]d\tau \tag{D10}$$

with $(\omega_m^{(\nu)}=\omega-\nu\omega_0)$. It follows from the above expression that envelope correlation matrices $C_s^{(\nu)}(\tau)$ only need to be evaluated for $\tau\geq 0$ and inserting Equation (D7) into Equation (D10) gives

$$S^{(\nu)}\left(\omega_m^{(\nu)}\right)=\frac{X_{s,\nu}^{*}X_{s,\nu}^{\top}-\Omega^{(\nu)}}{(0.5\omega_0^2\nu^2c)-j\omega_m^{(\nu)}}+\sum_{\rho}\sum_{l=2}^{k}\frac{\Theta_{l\rho}^{(\nu)}}{|\mu_{l,r}|+(0.5\omega_0^2\rho^2c)-j\left(\omega_m^{(\nu)}+\mu_{l,i}\right)}+\{\ldots\}^{\dagger} \tag{D11}$$

where the complex Floquet characteristic components were written $\mu_l=\mu_{l,r}+j\mu_{l,i}$ where $\mu_{l,r}\leq 0$ must hold to ensure stability of the PSS solution (see Section 2.3). Let $[M]_{(q,q)}$ denote the $q$th diagonal element of matrix $M$. We then write the $q$th diagonal element of the complex matrices in Equations (D8)–(D9) as $\left[\Omega_m^{(\nu)}\right]_{(q,q)}/\|X_{s,\nu}^{[q]}\|^2=a^{(\nu)}+jb^{(\nu)}$, $\left[\Theta_{l\rho}^{(\nu)}\right]_{(q,q)}/\|X_{s,\nu}^{[q]}\|^2=\Upsilon_{l\rho}^{(\nu)}+j\Delta_{l\rho}^{(\nu)}$. The $q$th diagonal element of the spectrum in Equation (D11) is then written

$$\left[S^{(\nu)}(\omega_m)\right]_{(q,q)}=\|X_{s,\nu}^{[q]}\|^2\left[\frac{(1-a^{(\nu)})(\omega_0^2\nu^2c)-2b^{(\nu)}\omega_m^{(\nu)}}{(0.5\omega_0^2\nu^2c)^2+\left(\omega_m^{(\nu)}\right)^2}+\sum_{\rho}\sum_{l=2}^{k}\frac{\Upsilon_{l\rho}^{(\nu)}\left[2|\mu_{l,r}|+(\omega_0^2\rho^2c)\right]+2\Delta_{l\rho}^{(\nu)}\left[\omega_m^{(\nu)}+\mu_{l,i}\right]}{\left(|\mu_{l,r}|+(0.5\omega_0^2\rho^2c)\right)^2+\left(\omega_m^{(\nu)}+\mu_{l,i}\right)^2}\right] \tag{D12}$$